Limnol. Oceanogr., 39(6), 1994, 1368–1398

The light field of microbenthic communities: Radiance distribution and microscale optics of sandy coastal sediments

Michael Kühl[1,2] *and Bo Barker Jørgensen*[2]
Department of Microbial Ecology, Institute of Biological Sciences, University of Aarhus, Ny Munkegade Bldg. 540, DK-8000C Aarhus, Denmark

Abstract

The light field in coastal sediments was investigated at a spatial resolution of 0.2–0.5 mm by spectral measurements (450–850 nm) of field radiance and scalar irradiance using fiber-optic microprobes. Depth profiles of field radiance were measured with radiance microprobes at representative angles relative to vertically incident collimated light in rinsed quartz sand and in a coastal sandy sediment colonized by microalgae. Upwelling and downwelling components of irradiance and scalar irradiance were calculated from the radiance distributions. Calculated total scalar irradiance agreed well with the scalar irradiance measured directly by a fiber-optic scalar irradiance microprobe. Close to the sediment surface, the light field was highly anisotropic, dominated by incident collimated light, and the scalar irradiance reached a maximum of 200% of incident scalar irradiance. Below the sediment surface, the light field became diffuse with a forward-biased angular light distribution. A few millimeters into the sediment surface, attenuation coefficients of field radiance, irradiance, and scalar irradiance became identical and independent of depth, indicating that the light field approached an asymptotic radiance distribution. Comparison of light fields in wet and dry quartz sand showed that the lower refractive index of air than of water caused a more forward-biased scattering in wet sand. Light penetration was therefore deeper and surface irradiance reflectance was lower in wet sand than in dry sand. The higher reflectance of dry sand resulted in a higher surface maximum of scalar irradiance. Asymptotic values of average cosines and attenuation coefficients were used to calculate the absorption coefficient in quartz sand and in a coastal sediment with diatoms. Absorption coefficients ranged from 2.5 mm^{-1} at 450 nm to 1.5 mm^{-1} at 850 nm in the coastal sediment and from 0.8 to 0.4 mm^{-1} in wet quartz sand. Both attenuation spectra and absorption spectra of the coastal sediment with diatoms exhibited a Chl *a* absorption maximum at 675 nm. The light field around microalgae in sediments differs strongly from the incident light field with respect to intensity and spectral composition.

Optical properties of aquatic ecosystems and interactions between the light field and photosynthetic microorganisms have mostly been studied in the water column of lakes and in the ocean (e.g. Jerlov 1976; Kirk 1983; Højerslev 1986; the December 1989 issue of *Limnology and Oceanography*). Hydrologic optics is thus a well-established discipline, and the analytical description and modeling of the light field in water has reached a high degree of accuracy (e.g. Preisendorfer 1976).

In comparison to pelagic systems, knowledge about the optical properties of microbenthic communities is limited. Light in microbenthic environments is subject to intense absorption and multiple scattering due to the much higher density of sediment particles and microalgae. High optical density results in a euphotic zone ranging from a few tenths of a millimeter to several millimeters deep (Jørgensen et al. 1983). Although it is a key parameter for microbenthic photosynthesis, few studies of light propagation in sediments have been made. Earlier studies mostly involved measurements of downwelling irradiance on a millimeter scale using a large cosine collector covered by increasing amounts of sediment material (Hoffmann 1949; Taylor 1964; Taylor and Gebelein 1966; Gomoiu 1967; Haardt

[1] Corresponding author.
[2] Present address: Max Planck Institute for Marine Microbiology, Fahrenheitstr. 1, D-28359 Bremen, Germany.

Acknowledgments

We thank Niels K. Højerslev and John T. O. Kirk for comments and suggestions, Carsten Lassen for providing fiber-optic scalar irradiance microprobes, and Dorthe Ganzhorn for technical assistance. We especially thank Leonid Fukshansky for constructive suggestions and discussions and for introducing us to the optics of heterogeneous multiple scattering media. We also thank two anonymous reviewers for suggestions and comments.

Financial support was provided by the Carlsberg Foundation (Denmark), the Danish Center for Environmental Biotechnology, the Danish Natural Science Research Council, and the Max Planck Society (Germany).

and Nielsen 1980). In other studies, a miniprobe was inserted into the sediment, demonstrating rapid light attenuation (Fenchel and Straarup 1971; Pierson et al. 1990). However, the light-collecting properties of these probes were not well defined, and the data could not therefore be related to specific optical parameters.

Introduction of fiber-optic microprobes with high spatial resolution and well-defined light-collecting properties demonstrated the significance of also analyzing scattered light when studying light propagation in optically dense media (Vogelmann and Björn 1984; Jørgensen and Des Marais 1986; Star et al. 1987; Lassen et al. 1992*a*; Kühl and Jørgensen 1992). With these techniques, scattered light in plant and animal tissue and in cyanobacterial mats was analyzed by field radiance measurements at different angles relative to a collimated light source (Vogelmann and Björn 1984; Jørgensen and Des Marais 1988). The radiance data were then used to calculate scalar irradiance (i.e. the integral of radiance incident from all directions around a point in space). Because scalar irradiance is also a measure of the total quantum flux to single algal cells, it is the most relevant parameter in relation to photosynthesis and other photobiological processes in turbid media (Smith and Wilson 1972).

A fiber-optic microprobe for direct measurements of scalar irradiance at a spatial resolution of <100 μm was recently developed (Lassen et al. 1992*a*). This probe makes it possible to relate microscale measurements of oxygenic photosynthesis to the light field in microbenthic communities by the combined use of oxygen microelectrodes and fiber-optic scalar irradiance microprobes (Revsbech and Jørgensen 1983; Lassen et al. 1992*b*; Kühl and Jørgensen 1992). Both the calculated and the directly measured spectral scalar irradiance differ significantly in spectral composition from the incident irradiance and have a surface or subsurface maximum of up to $\sim$200% of the incident downwelling scalar irradiance (Jørgensen and Des Marais 1988; Lassen et al. 1992*b*; Kühl and Jørgensen 1992; Kühl et al. 1994*a*,*b*). Because the benthic microalgae are thus exposed to light of different intensity and spectral composition than the light source, direct microscale measurements of the spectral light field are required.

In this study, we present detailed microscale radiance measurements of the angular structure of the light field in sediments with different scattering and absorption characteristics. Angular radiance distributions were used to calculate optical parameters describing the light field. Calculated scalar irradiance was also compared to scalar irradiance measured directly with a fiber-optic microprobe.

The goals were to characterize the basic properties of the light field in uniform coastal sediment layers, analyze the physical mechanisms behind the optical properties of sediments, and introduce a conceptual background of microscale optics in sediments for ecological studies of microbenthic photosynthesis, phototactic movements, and other photobiological processes. Similar studies of more complex light fields in optically laminated microbenthic communities (e.g. microbial mats and biofilms) are presented elsewhere (Kühl et al. 1994*b*).

Methods

Sediment types—Two different types of coastal sediment were investigated. Quartz sand was collected from the upper littoral zone at a beach near Rønbjerg, Limfjorden, Denmark. The sediment was sieved into different particle-size fractions, and animals and organic material adherent to the sand grains were removed by washing. The sediment was dried at 105°C. Sand with a grain size of 125–250 μm was chosen for radiance distribution measurements.

Another coastal sediment was collected from below the tidal zone at a water depth of 0.5 m at Aggersund, Limfjorden. The upper 0–1.5 cm was dark brown and consisted of a homogeneous mixture of sand grains, diatoms, and amorphous organic material. Sediment was collected in small Plexiglas coring tubes, and the upper 0–1 cm was used for light measurements after careful removal of animals by forceps under a dissection microscope. The grain-size distribution of the sediment was dominated by sand grains 63–250 μm in diameter which were overgrown by pennate diatoms, mostly *Nitzschia* sp. and *Navicula* sp.

Experimental setup—Light measurements were done in 7–8-mm-thick sediment samples transferred to small coring tubes (12–15 mm high, 42-mm diam); the tubes were painted

black and sealed at the bottom with a plug of solidified agar (1.5% wt/wt). Measurements in wet quartz sand and in coastal sediment with diatoms were done with 3–5 mm of seawater on top of the sediment. The cores were placed on a black Petri dish with a 5–mm hole in it; the hole allowed penetration of the sediment sample from below, through the agar plug. A fiber-optic tungsten-halogen light source (Schott KL-1500) with a collimating lens was used for homogeneous illumination of sediment samples vertically from above. We avoided lateral light gradients by illuminating a large area of sediment relative to the depth of light penetration. Optical alignment was done by measuring downwelling radiance at 0° zenith angle without a sediment sample in the light path, which ensured illumination normal to the sediment surface. Experiments were performed in a dark room, and stray light was minimized by covering all reflecting surfaces with black cloth and tape and by enclosing the whole setup with black cloth. Microscale spectral light measurements (450–850 nm) for field radiance and scalar irradiance were made at a spatial resolution of 0.2–0.5 mm by fiber-optic microprobes connected to an optical spectral multichannel analyzer (O-SMA, Kühl and Jørgensen 1992). The fiber-optic microprobes were inserted into the sediment samples by a micromanipulator with a specified accuracy of ±5 μm (Märtzhäuser).

Radiance measurements—Field radiance, i.e. the light from a defined direction (*see list of notation for light field parameters*), was measured by a fiber-optic microprobe with a tip diameter of 125 μm and a narrow and well-defined acceptance cone (numerical aperture, NA = 0.2) (Kühl and Jørgensen 1992). The acceptance half-angle was 11.5° in air and 8.6° in water. Depth profiles of spectral downwelling radiance were measured at 0° zenith angle by penetrating the sediment sample from below through the agar plug. Micromanipulator readings were related to actual depths below the sediment surface by positioning the fiber probe at the sediment surface and then lowering it a known vertical distance into the sediment. Before each measurement of depth profiles, the sediment sample was vibrated slightly in order to collapse possible light channels created by the fiber probe. The surface position of the fiber-optic probe was determined by observation through a dissection microscope.

Depth profiles of forward-scattered radiance were measured with the same technique by penetrating the sediment sample from below at zenith angles of 20°, 40°, and 60° relative to the incident collimated light. Depth profiles of backscattered radiance were measured by penetrating the sediment from above at zenith angles of 120°, 140°, and 160°. The absolute distance travelled by the micromanipulator was adjusted for each angle to ensure measurements at the same vertical distance from the sediment surface. Values for radiance at zenith angles of 80° and 100° were estimated by interpolation between measured field radiance at 60° and 120°, whereas radiance at 180° was estimated by extrapolation from measurements at 140° and 160°. Thus, all zenith angles from 0° to 180° were covered at 20° intervals, corresponding to the acceptance angle of the fiber-optic probe.

Scalar irradiance measurements—Depth profiles of scalar irradiance spectra were measured directly in wet sand (125–250 μm) with a fiber-optic microprobe for scalar irradiance; the probe had an isotropic response and a tip diameter of 80 μm (Lassen et al. 1992*a*). The scalar irradiance probe was inserted into the sediment at a zenith angle of 135° relative to the incident light. Scalar irradiance measurements were related to the incident light by measuring the downwelling scalar irradiance over a black light well as described by Lassen et al. (1992*a*).

Theory and calculations

All optical parameters discussed here are assumed functions of the wavelength of light. Wavelength is therefore not delineated in the nomenclature and definitions of optical parameters (lists of notation for light field parameters and inherent optical parameters are provided). The nomenclature follows recommendations by the Working Group of the International Association of the Physical Sciences of the Ocean (IAPSO 1985).

Radiance calculations—The field radiance, $L(\theta, \phi)$, from a given direction is the radiant flux, Φ, per unit solid angle, ω, per unit area, A, at right angles relative to the direction of propagation specified by the zenith angle, θ,

and the azimuth angle, ϕ, in a spherical coordinate system (Fig. 1) (Kirk 1983):

$$L(\theta, \phi) = d^2\Phi/dA\, d\omega. \quad (1)$$

The field radiance distribution solid over all directions thus forms a unit sphere of 4π solid angle. Light penetration into sediments has mostly been measured as the downwelling irradiance, E_d, which is a measure of the total radiant flux incident from the upper hemisphere per unit area of a horizontal surface element (Fig. 1):

$$E_d(z) = \int_{2\pi} L(z; \theta, \phi)\cos\theta\, d\omega. \quad (2)$$

Upwelling irradiance, E_u, is a measure of the total upwelling radiant flux from the lower hemisphere per unit area of horizontal surface element:

$$E_u(z) = \int_{-2\pi} L(z; \theta, \phi)|\cos\theta|\, d\omega. \quad (3)$$

In most natural waters, the upwelling irradiance is only a few percent of the downwelling light (Kirk 1983). This is, however, not the case in sediments, where the high concentration of particulate matter results in intense backscattering (Jørgensen and Des Marais 1988; Pierson et al. 1990). The large contribution of scattered light in sediments therefore makes irradiance a less suitable parameter for studies of light and photosynthesis in microbenthic communities where microalgal cells receive scattered light from all directions (Kühl and Jørgensen 1992). The most relevant light parameter in relation to photosynthesis is here the scalar irradiance, E_0, i.e. the integral of the radiance distribution over all directions about a given point (Fig. 1):

$$E_0(z) = \int_{4\pi} L(z; \theta, \phi)\, d\omega = E_{0d} + E_{0u}. \quad (4)$$

The scalar irradiance has a downwelling component, E_{0d}, and an upwelling component, E_{0u}, which are derived by integration of the radiance distribution over the upper and lower hemispheres. We calculated irradiance and scalar irradiance from measurements of field radiance, $L(z; \theta')$, at a number of discrete zenith angles, θ'. We used a numerical integration

Fundamental optical parameters

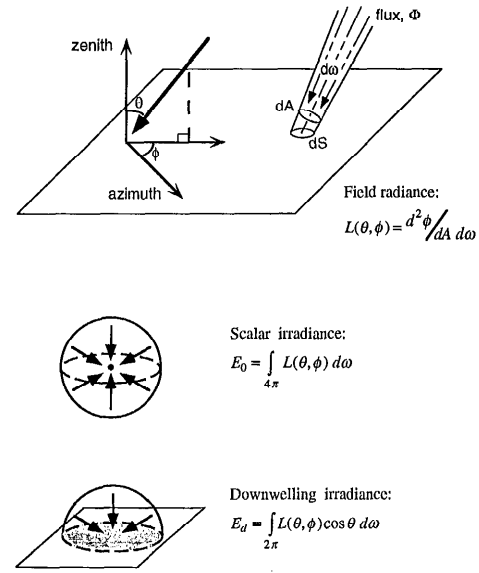

Fig. 1. The field radiance, $L(\theta, \phi)$, is the energy or quantum flux within the solid angle, $d\omega$, through an area, dA, perpendicular to the flux. Direction of light propagation is described in a spherical coordinate system by the spherical coordinates θ and ϕ, whereas $d\omega$ and dA represent infinitesimal quantities of solid angle and area. The radiance per unit horizontal surface, dS, integrated over the upper hemisphere (solid angle = 2π) is the downwelling irradiance, E_d. Note that irradiance weights the radiance with the cosine of its incident zenith angle, θ, and is a measure of the total downwelling radiant flux through a plane. Scalar irradiance, E_0, is the radiance integrated over the whole unit sphere (solid angle = 4π) and is a measure of the total radiant flux incident from all directions about a point (partly redrawn from Jørgensen 1989).

method originally described by Tyler et al. (1959) for radiance distributions in water and later by Vogelmann and Björn (1984) and Jørgensen and Des Marais (1988) for calculations of scalar irradiance in plant tissue and cyanobacterial mats.

The light field in the sediment was assumed to exhibit axial symmetry around the vertically incident collimated light (Jørgensen and Des Marais 1988). Each radiance measurement at zenith angle, θ', relative to the light source covered an angular interval, $\Delta\theta'$, of $\pm 10°$ around the direction of measurement and was thus representative of a spherical band as wide as

Notation for light field parameters in sediments

$L(z; \theta, \phi)$	Field radiance—the radiant flux at depth z in a defined direction specified by the zenith angle, θ, and the azimuth angle, ϕ, in a spherical coordinate system per unit solid angle per unit area at right angles to the direction of propagation, W m^{-2} sr^{-1}
$E_d(z)$, $E_u(z)$	Downwelling and upwelling irradiance—the total radiant flux incident from the upper or lower hemisphere per unit area of a horizontal infinitesimally small surface element at depth z, W m^{-2} $$E_d(z) = \int_{2\pi} L(z; \theta, \phi)\cos\theta \, d\omega$$ $$E_u(z) = \int_{-2\pi} L(z; \theta, \phi)\cos\theta \, d\omega$$
$\mathbf{E}(z)$	Downwelling vector irradiance—the net downwelling radiant energy at depth z, W m^{-2} $$= \int_{4\pi} L(z; \theta, \phi)\cos\theta \, d\omega = E_d(z) - E_u(z)$$
$E_0(z)$	Scalar irradiance—the integral of the radiance distribution over all directions about a point at depth z, W m^{-2} $$= \int_{4\pi} L(z; \theta, \phi) \, d\omega = E_{0d}(z) + E_{0u}(z)$$
$E_{0d}(z)$, $E_{0u}(z)$	Downwelling and upwelling scalar irradiance—the integral of the radiance distribution over the lower or upper hemisphere at a point at depth z, W m^{-2} $$E_{0d}(z) = \int_{2\pi} L(z; \theta, \phi) \, d\omega$$ $$E_{0u}(z) = \int_{-2\pi} L(z; \theta, \phi) \, d\omega$$
$K_{L(\theta,\phi)}$	Vertical attenuation coefficient of radiance, mm^{-1} $$= -\frac{\mathrm{d} \ln L(\theta, \phi)}{\mathrm{d}z} = -\frac{1}{L(\theta, \phi)} \frac{\mathrm{d}L(\theta, \phi)}{\mathrm{d}z}$$
K_d, K_u, $K_{\mathbf{E}}$, $K_{E_{0d}}$, $K_{E_{0u}}$, K_{E_0}	Diffuse vertical attenuation coefficients of irradiance or scalar irradiance components, mm^{-1} $$K = -\frac{\mathrm{d} \ln E}{\mathrm{d}z} = -\frac{1}{E}\frac{\mathrm{d}E}{\mathrm{d}z}$$
$R(z)$	Irradiance reflectance—the ratio of upward to downward irradiance at depth z $$= E_u(z)/E_d(z)$$
$\mu(z)$	Average cosine—the mean cosine of the average path direction (zenith angle) of both upwelling and downwelling photons at depth z $$= \frac{\int_{4\pi} L(z; \theta, \phi)\cos\theta \, \mathrm{d}\omega}{\int_{4\pi} L(z; \theta, \phi) \, \mathrm{d}\omega} = \frac{\mathbf{E}(z)}{E_0(z)} = \frac{E_d - E_u}{E_0}$$
$\mu_d(z)$	Downwelling average cosine—the mean cosine of the average path direction (zenith angle, θ) travelled by downwelling photons at depth z $$= \frac{\int_{2\pi} L(z; \theta, \phi) \cos\theta \, \mathrm{d}\omega}{\int_{2\pi} L(z; \theta, \phi) \, \mathrm{d}\omega} = \frac{E_d(z)}{E_{0d}(z)}$$
$\mu_u(z)$	Upwelling average cosine—the mean cosine of the average path direction (nadir angle, $\theta_n = 180° - \theta$) travelled by upwelling photons at depth z $$= \frac{E_u(z)}{E_{0u}(z)}$$
K_a, R_a, μ_a, μ_{da}, μ_{ua}	Asymptotic values for diffuse attenuation coefficient, irradiance reflectance, down- and upwelling average cosine, and total average cosine

Notation for inherent optical parameters of sediments

a Absorption coefficient—the fraction of an incident beam of light which is absorbed by and infinitesimally thin layer of sediment, mm $^{-1}$

$\beta(\Phi)$, or $\beta(\theta, \phi; \theta', \phi')$
Volume scattering function—the radiant intensity scattered at a given angle (Φ) from the original direction of propagation (θ, ϕ) into the new direction (θ', ϕ') per unit irradiance per unit volume of an infinitesimally small volume of sediment, mm^{-1} sr^{-1}

b Total scattering coefficient—the fraction of an incident beam of light which is diverted out of the incident light path by an infinitesimally thin layer of sediment, mm^{-1}

$$= 2\pi \int_0^{\pi} \beta(\Phi)\sin \Phi \, d\Phi = \int_{4\pi} \beta(\Phi) \, d\omega$$

$c = a + b$
Beam attenuation coefficient—the fraction of an incident beam of light which is lost due to the combined action of absorption and scattering in an infinitesimally thin layer of sediment, mm^{-1}

ω_0 Single scattering albedo—the fraction of incident photons redistributed as scattered light by a single particle encounter

$$= b/c$$

μ_s Average cosine of scattering—the cosine of the mean angle of scattering relative to the original light path of incident photons by a single particle encounter

$$= \frac{\int_{4\pi} \beta(\Phi)\cos \Phi \, d\omega}{\int_{4\pi} \beta(\Phi) \, d\omega}$$

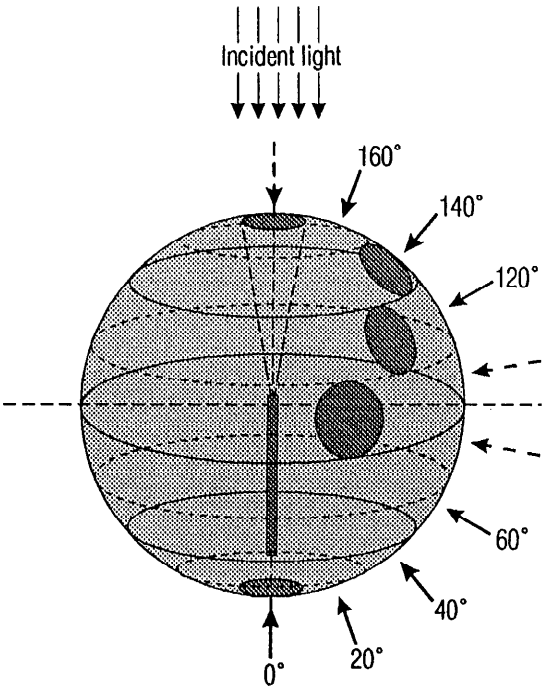

Fig. 2. Schematic illustration of the technique used to integrate field radiance distributions in sediments. Solid arrows indicate the zenith angles where depth profiles of field radiance were measured. At 0° zenith angle the optical fiber points directly toward the light source. Dashed arrows indicate the zenith angles at which radiance values were calculated by interpolation or extrapolation. The fiber-optic radiance probe covered an angular interval of about ±10° around each measuring direction and the measured value was taken as being representative for all azimuth angles due to axial symmetry around the vertical illumination.

the acceptance cone of the optical fiber (Fig. 2). This procedure is equivalent to taking the radiance measured at a given zenith angle and rotating the projection of the acceptance cone on the radiance distribution solid around the vertical axis (Jørgensen and Des Marais 1988). We did this numerically by multiplying the measured radiance at each direction with a weighting factor, $W(\theta')$, which is the surface area of the spherical zone on the unit sphere (radius = 1) and which is determined by the interval of zenith angle, $\Delta\theta'$, around the measuring angle, θ', relative to the incident light:

$$W(\theta') = 2\pi|\cos(\theta' + \Delta\theta') - \cos(\theta' - \Delta\theta')|. \quad (5)$$

The sum of all weighting factors equals 4π (i.e. the surface area of the unit sphere, Table 1). We obtained radiance data for 10 angular intervals of ±10° zenith angle covering all zenith angles from 0° to 180°. Thus, irradiance was calculated as

$$\Sigma W(\theta')L(z; \theta')\cos \theta'; \; 0° \leq \theta' \leq 180°. \quad (6)$$

Scalar irradiance was calculated as

$$\Sigma W(\theta')L(z; \theta'); \; 0° \leq \theta' \leq 180°. \quad (7)$$

Upwelling and downwelling components of irradiance and scalar irradiance were calculated from Eq. 6 and 7 by summation over measured zenith angles covering the upper and lower hemisphere.

Attenuation coefficients—The attenuation coefficients of radiance, irradiance, and scalar irradiance (*see notation for light field parameters*) were calculated over a depth interval in the sediment:

Table 1. Weighting factors, $W(\theta')$, for numerical integration of radiance values measured at 10 different zenith angles. Each measurement is representative for a spherical zone of ±10° zenith angle around the measuring angle, θ', relative to the vertically incident light.

Light-fiber angle, θ'	Spherical zone, $\theta' \pm \Delta\theta'$	Weighting factor, $W(\theta')$
0° and 180°	0°–10° and 170°–180°	0.095 (×2)
20° and 160°	10°–30° and 150°–170°	0.746 (×2)
40° and 140°	30°–50° and 130°–150°	1.403 (×2)
60° and 120°	50°–70° and 110°–130°	1.890 (×2)
80° and 100°	70°–90° and 90°–110°	2.149 (×2)
Sum	0°–180°	12.566 (=4π)

$$K = \ln(E_1/E_2)/(z_2 - z_1). \quad (8)$$

E_1 and E_2 are the values of the parameter of interest at depths z_1 and z_2.

Average cosines—The radiance distribution gives a complete picture of the angular structure of the light field but consists of large amounts of data which are difficult to obtain experimentally. A simpler measure of the angular light distribution is the average cosine, μ, and its upwelling and downwelling components, μ_u and μ_d, which can be calculated from measurements of scalar irradiance and irradiance.

μ is the mean cosine of the average path direction (zenith angle) of all up- and downwelling photons at a certain depth horizon and is calculated as the ratio of net downwelling irradiance, i.e. the vector irradiance, $\mathbf{E} = (E_d - E_u)$, and the scalar irradiance, E_0 (*see notation for light field parameters*). In the case of a perfectly collimated light field (no scattering), the average cosine would equal 1, whereas an isotropic light field with equal amounts of up- and downwelling photons would have an average cosine of zero. In light-scattering media the average cosine is an integral measure of the angular structure of the total light field. Analogous parameters describing the angular structure of the downwelling and upwelling parts of the light field are μ_d and μ_u (*see notation for light field parameters*).

The reciprocals of μ_d and μ_u are also called the distribution functions of downwelling and upwelling light because they can be interpreted as a measure of the mean pathlength per vertical distance traversed by the downwelling or upwelling flux of photons per unit horizontal area per second (Kirk 1991). For a perfectly isotropic distribution of light, the mean pathlength travelled by up- or downwelling photons through an infinitesimally thin sediment layer is exactly twice the geometrical thickness of the layer, i.e. the vertical distance travelled by photons that have not been scattered (Kortüm 1969). Thus, μ_u or μ_d become equal to 0.5 in an isotropic light field.

Irradiance reflectance—The irradiance reflectance, R, is the ratio of upwelling irradiance to downwelling irradiance (*see light field parameters*) and is thus a measure of the relative amount of backscattered light in the sediment. In the case of no scattering, $R = 0$, whereas irradiance reflectance becomes 1 for a surface acting as a perfect mirror (no absorption). Thus, $0 < R < 1$ in sediments. The irradiance reflectance at a boundary between two media of different refractive index (e.g. the sediment–water or sediment–air interface) is also called the albedo and includes both diffuse backscattered light and light reflected due to the difference in refractive index.

Light field parameters and inherent optical parameters—In the following, we discriminate between optical properties of the light field (i.e. optical parameters that change with the angular structure of the light field) and optical properties of the medium (which for a given incident light field determine the angular light field in sediments but are not dependent on it). Irradiance, scalar irradiance, and derived parameters are all determined by the radiance distribution in sediments and will be designated light field parameters. The shape of a measured radiance distribution in a sediment for a given incident light field is, however, determined by the inherent optical properties of the sediment and the medium surrounding it, i.e. the absorption coefficient, a, the scattering coefficient, b, and the volume scattering function, $\beta(\Phi)$ (*see notation for inherent optical parameters*).

Attenuation of light is caused by the combined effect of absorption and scattering and is quantified as the beam attenuation coefficient, $c = a + b$. The attenuation coefficient specifies the probability of a photon travelling a certain distance in a direction before being absorbed or scattered out of the light path (Kirk

1981). The reciprocal of the attenuation coefficient, $1/c$, is called the mean free path and is a measure of the average distance travelled by a photon before a scattering or absorption event (Wilson and Jaques 1990). The volume scattering function, $\beta(\Phi)$, then specifies the probability for scattering of a photon out of the light path at a certain angle, Φ, relative to the original light path direction (i.e. the angular distribution of single-event scattering).

Radiative transfer theory—The mathematical analysis and modeling of the light field in scattering media has been a matter of intensive research for many years (e.g. Gershun 1939; Preisendorfer 1976; Ishimaru 1978). If we assume that sediments can be described as plan-parallel media, it is possible to relate the variation of radiance along a given direction in a sediment to the inherent optical parameters of that sediment. This relation is formulated in the *equation of radiative transfer* for a plan-parallel medium (Preisendorfer 1976; Ishimaru 1978):

$$\cos\theta \frac{\mathrm{d}L(z;\theta,\phi)}{\mathrm{d}z} = -c(z)L(z;\theta,\phi) + L^*(z;\theta,\phi) + F^*(z;\theta,\phi), \quad (9)$$

which states that the net rate of change in radiance over the distance $r = z/\cos\theta$ along a direction specified by the spherical coordinates θ and ϕ at the vertical depth z (left-hand term of Eq. 9) is determined by the loss of light out of the light path by absorption and scattering $[-c(z)L(z;\theta,\phi);\ c(z) = a(z) + b(z)]$, the gain of light scattered into the light path from other directions $[L^*(z;\theta,\phi)]$, and light resulting from fluorescence or bioluminescence in the sediment $[F^*(z;\theta,\phi)]$. The fluorescence term will not be considered in the following because the density of fluorescent material (i.e. microalgae) was relatively low in the investigated sediments. Fluorescence may, however, be important in densely populated phototrophic communities such as microbial mats and phototrophic biofilms.

The mathematical treatment of Eq. 9 is difficult because of the complex shape of observed radiance distributions and volume-scattering functions in scattering media (e.g. Ashley and Cobb 1958; Isacchi and Lenoble 1959; Kullenberg 1972) which cannot be described by an exact mathematical formalism (Jerlov 1976; Kirk 1981). Several relations between light field parameters and inherent optical parameters have, however, been formulated for light propagation in both water and plant and animal tissue by application of numerical methods like Monte Carlo simulation, multiflux models, and diffusion approximations (e.g. Ishimaru 1978, 1989; Kirk 1981; Fukshansky et al. 1991; Cheong et al. 1990; Profio 1989). Similar models have not yet been applied to sediments.

Absorption coefficient—A simple relation between the absorption coefficient, a, the vector irradiance, $\mathbf{E}$, and the scalar irradiance, E_0, can be derived directly by integrating Eq. 9 (ignoring the term for internal sources, eg. fluorescence) over all angles of light propagation, yielding *Gershun's equation* (Gershun 1939):

$$\frac{\mathrm{d}\mathbf{E}}{\mathrm{d}z} = -cE_0 + bE_0 = -aE_0. \quad (10)$$

The vector irradiance, $\mathbf{E} = E_d - E_u$, is a measure of the net downwelling irradiance. The absorption coefficient can thus be calculated as

$$a = K_{\mathbf{E}}\frac{\mathbf{E}}{E_0} = K_{\mathbf{E}}\mu. \quad (11)$$

$K_{\mathbf{E}}$ is the attenuation coefficient of vector irradiance. Equation 11 is valid in homogeneous, nonfluorescing media with constant refraction indices. Whether sediments fulfill these requirements is discussed later.

Scattering theory for large particles—Coastal sediments are composed of particles with high density and a mixture of sizes—generally large relative to the wavelength of light. Due to the high density of particles, the angular light field (and thus light propagation in sediments) is the result of multiple encounters between photons and sediment particles (i.e. multiple scattering and absorption).

Single-event scattering of light by particles that are small or comparable in size to the wavelength of light can be described in terms of the wave properties of light [i.e. electromagnetic theories like isotropic Rayleigh scattering (size $\ll$ wavelength) and anisotropic Mie-scattering (size $\sim$ wavelength)]. However,

single-event light scattering by large particles (>10–20 times the wavelength of light) can be described in terms of geometrical optics (van de Hulst 1957; Hodkinson and Greenleaves 1963).

The scattering properties of a single particle are determined by its size, shape, and refractive index relative to the surrounding medium. The refractive index determines the optical effective size $[(n - n_0)/n_0]d$, where d is the particle diameter, n is the particle refractive index, and n_0 is the refractive index of the surrounding medium (van de Hulst 1957). Thus, a particle with a high refractive index relative to the surrounding medium has an optical effective size larger than its geometrical size. For large nonabsorbing particles (>10–20 times the wavelength of light), the amount of incident light redistributed as scattered light becomes independent of refractive index and approaches an asymptotic value of $2\pi r^2 E$, where r is the particle radius, and E is the incident irradiance, i.e. 2× the geometrical cross-section of the particle (van de Hulst 1957; Twomey et al. 1986).

Sediments are, however, composed of colored particles which absorb some of the incident light. Thus, after an encounter with a particle, only a fraction of incident photons will be re-emitted as scattered light. A measure of the scattering efficiency is the single-scattering albedo of a particle, ω_0, which is defined as the ratio of the scattering coefficient and the attenuation coefficient: $\omega_0 = b/c$. The remaining fraction $(1 - \omega_0)$ is thus a measure of particle absorption efficiency. For sand grains and other particulate components of sediments, the single-scattering albedo is high ($\omega_0 > 0.9$) throughout the spectrum of light (Twomey et al. 1986). This may, however, not be true for microalgae and organic debris, which exhibit high absorption at specific wavelengths of light.

The angular distribution of scattered light is determined by the particle size as well as the refractive index of the particle and the surrounding medium. Scattering by large particles is caused by reflection and refraction as well as diffraction of light and results in a predominantly forward-directed angular distribution of scattered light at small angles around the original direction of incident light (van de Hulst 1957; Ashley and Cobb 1958). Whereas scattering due to refraction and reflection depends on the refraction index and has a more diffuse forward-biased angular distribution (scattering angles >10°), diffraction is independent of particle composition, only depends on the size and shape of the particles, and is always strongly forward directed (scattering angles from 0° to 10–15°) (Hodkinson and Greenleaves 1963). Thus, single-event scattering by particles in sediments is anisotropic with a complex angular distribution of the scattered light, i.e. a complex volume scattering function, $\beta(\Phi)$. The degree of anisotropy of single-event particle scattering is described by the average cosine of scattering, μ_s, and is defined in terms of the volume scattering function, $\beta(\Phi)$ (Ishimaru 1989; Kirk 1991):

$$\mu_s = \frac{\int_{4\pi} \beta(\Phi)\cos\Phi \, d\omega}{\int_{4\pi} \beta(\Phi) \, d\omega}. \qquad (12)$$

Values of μ_s range from backwardly peaked ($-1 < \mu_s < 0$) via isotropical ($\mu_s = 0$) to forwardly peaked scattering ($0 < \mu_s < 1$) (Groenhuis et al. 1983). The closer the refractive index of a particle matches the refractive index of the surrounding medium, the more forward directed the angular distribution of scattered light will be, i.e. μ_s gets closer to 1 (Twomey et al. 1986). This effect of refractive index will only affect the component of scattering caused by reflection and refraction. Thus, the largest effects of a change in the refractive index of the surrounding media would be observed at scattering angles >10°–15°.

Results

We present data for both single wavelengths and for whole spectra. Recorded spectra in the rinsed quartz sand and in the coastal sediment with diatoms exhibited only relatively weak spectral details. Calculations were therefore done at a few selected wavelengths covering the spectral range of 450–850 nm. Presented values of radiance, irradiance, and scalar irradiance were normalized to the incident light at the sediment surface and are thus expressed in relative units as percentages of surface downwelling radiance at 0° or downwelling scalar irradiance.

Depth profiles of field radiance—The depth

distribution of field radiance for 650-nm light in dry and wet quartz sand and in coastal sediment with diatoms is shown for three different zenith angles in Fig. 3. Although the attenuation of light differed, all three sediments exhibited the same overall changes in light distribution with depth. Downwelling field radiance at 0° rapidly decreased from 100% to <1% of the surface value over the upper 0–1 mm of the sediment. Over the same depth interval, forward-scattered light measured at 40° increased from a very low surface value to a maximum at 0.5–1 mm below the sediment surface. At 40° angle, the collimated light source was outside the acceptance cone of the optical fiber and only forward-scattered light was detected. Highest values of forward-scattered light at the very surface were found in wet quartz sand (0.2% of surface radiance at 0°), whereas both dry sand and the diatom sediment exhibited values of forward-scattered light at the sediment surface that were ~4 orders of magnitude lower than 0° downwelling radiance. Forward-scattered light in the sediments was most intense in the wet quartz sand, where it reached the same intensity as 0° downwelling radiance at 1 mm below the sediment surface (Fig. 3B). In dry sand and in the diatom sediment, levels of forward-scattered light were lower than 0° downwelling radiance throughout the sediment (Fig. 3A,C).

Attenuation of backscattered light measured at 140° was lowest in the upper 0.5–1 mm. Lowest levels of backscattered light from the sediment surface were found in the diatom sediment where they were more than three orders of magnitude lower than downwelling radiance at 0° (Fig. 3C). More backscattered light was found at the sediment surface of dry sand than of wet quartz sand (Fig. 3A,B). From a depth of 0.5–1 mm below the surface and throughout the sediment, backscattered light was between one and two orders of magnitude lower than 0° downwelling radiance measured at the same depths.

Below 1 mm, attenuation of field radiance became exponential with depth ($r^2 > 0.98$), with the same attenuation coefficient of radiance at all three zenith angles as indicated by the parallel and log-linear parts of the depth profiles in Fig. 3. Depth profiles of radiance measured at other zenith angles (data not shown) also exhibited an exponential attenu-

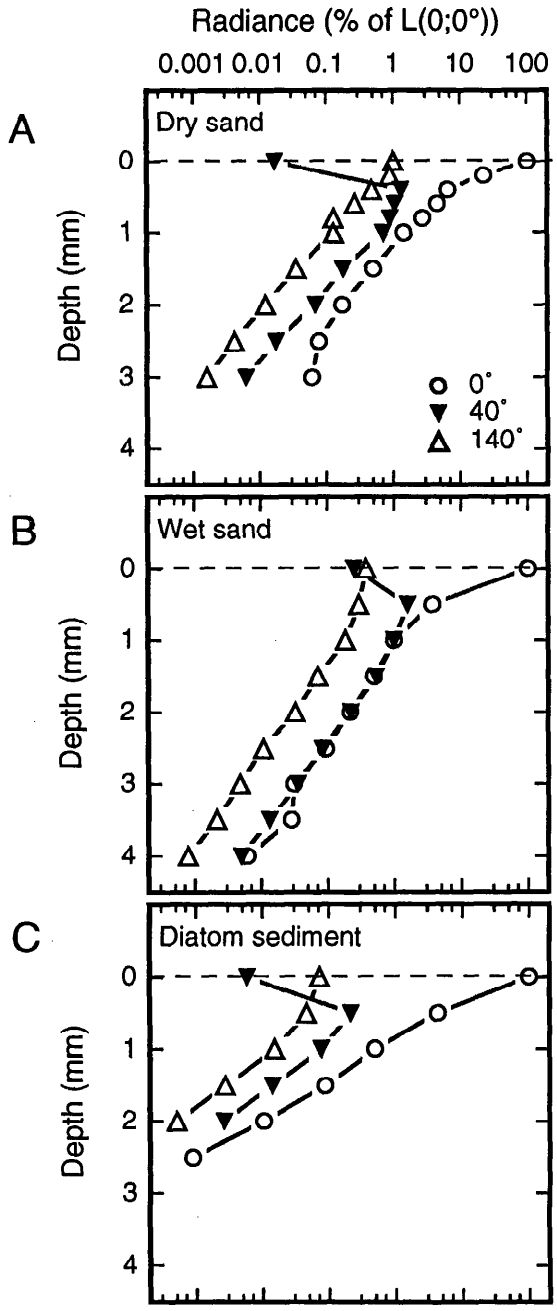

Fig. 3. Depth profiles of field radiance $L(z; \theta, \phi)$, at 650 nm in three types of sediment. A, B. Dry and wet quartz sand with a grain size of 125–250 μm. C. Sandy coastal sediment with diatoms. All data were normalized to incident 0° radiance at the sediment surface and are expressed on a logarithmic scale. Data represent the geometric mean of 2–5 measurements.

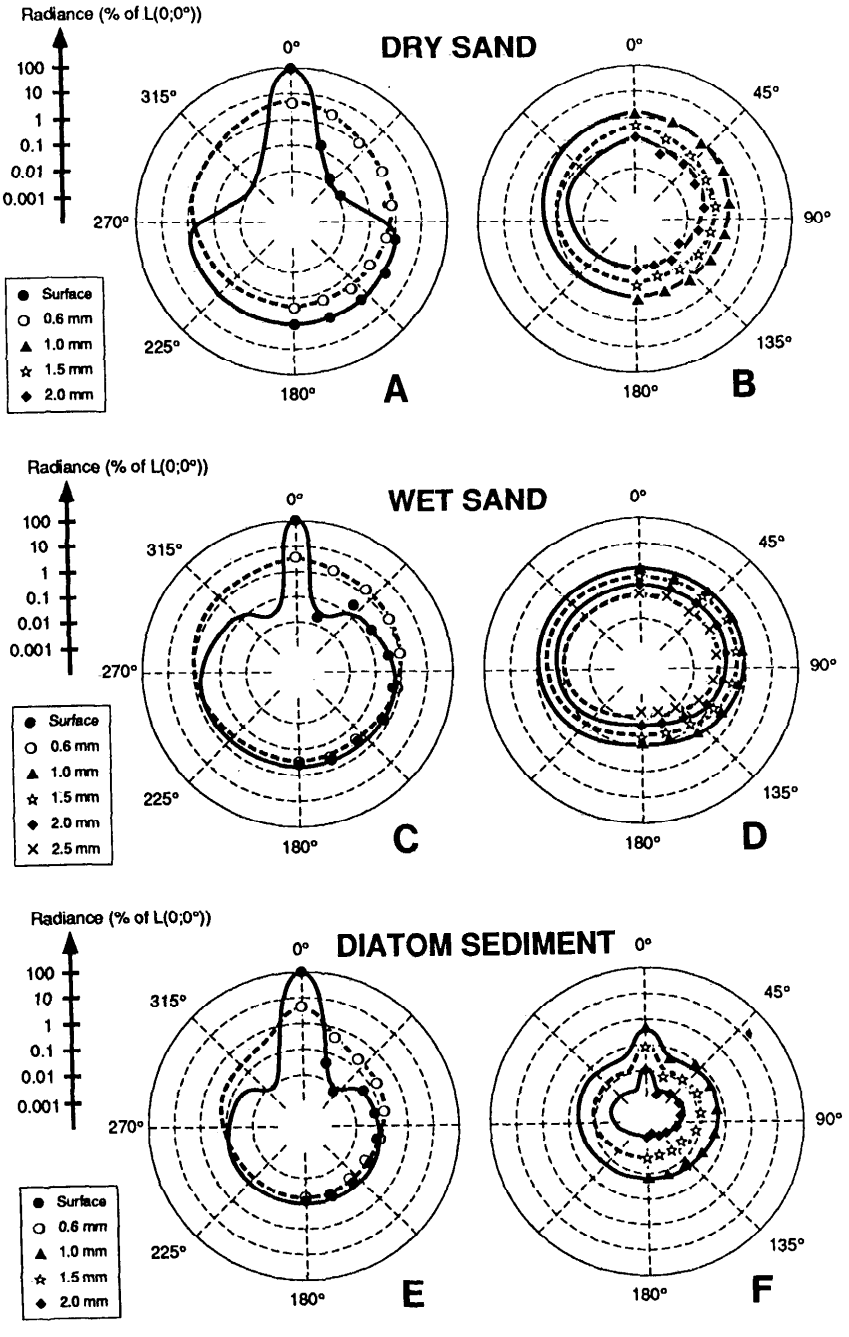

Fig. 4. Polar plots of the field radiance distribution, $L(z; \theta, \phi)$, for 650-nm light at different depths in three types of sediments. All data were normalized to incident 0° radiance at the sediment surface and are presented on a logarithmic scale vs. the corresponding zenith angle in a polar coordinate system. Although measurements covered only 0–180° zenith angles, curves were drawn as mirror images also for 180–360° because the light field is symmetrical around the vertical axis. Keys on figure panels indicate depth below the sediment surface. Data represent the geometric mean of 2–5 measurements.

ation of light below 1 mm from the sediment surface with a radiance attenuation coefficient, K_L, which was independent of zenith angle.

In general, light was most strongly attenuated in the diatom sediment [Fig. 3C; K_L (diatom) = 3.42±0.24 mm^{-1}], whereas dry sand attenuated light more strongly than wet sand did [Fig. 3A,B; K_L (dry) = 2.32±0.18 mm^{-1}, K_L (wet) = 1.75±0.12 mm^{-1}].

Radiance distribution—The total light field and its changes with depth in the investigated sediments are shown in Fig. 4, where the measured field radiance of 650-nm light was plotted against zenith angle in a polar coordinate system. Each curve corresponds to the radiance distribution at a certain depth in the investigated sediments.

At the sediment surface (solid line in Fig. 4A,C,E), the light field was highly anisotropic and was dominated by incident collimated light at 0° zenith angle, at which radiance was 10,000-fold higher than it was at 20–40° angle. Whereas only very low levels of diffuse forward-scattered light were detected at the sediment surface of dry quartz sand (Fig. 4A), forward-scattered light from zenith angles between 20° and 80° contributed significantly to the downwelling light at the sediment surface when the sand was covered by a water film (Fig. 4C). The same effect, though less pronounced, was observed at the surface of the diatom sediment, which also had much less backscattered light because of higher light absorption (Fig. 4E). Another important component of the light field was backscattered light from the sediment surface measured at zenith angles >90°. Backscattered light exhibited an almost isotropic distribution at the sediment surface (i.e. the radiance of backscattered light was the same at all zenith angles >90°).

Just below the sediment surface, a steep increase of diffuse forward-scattered light was observed, while downwelling 0° radiance and backscattered light (zenith angles >90°) decreased relative to the surface value (dashed line in Fig. 4A,C,E). The overall radiance distribution thus became more isotropic with a dominance of forward-scattered light. Below 1 mm from the sediment surface, the angular light field did not change much with depth and thus approached an asymptotic radiance distribution (Fig. 4B,D,F). The attenuation of light therefore became almost independent of the zenith angle below 1-mm depth. This depth corresponded to the depth below which all radiance profiles in Fig. 3 exhibited an exponential decrease with depth and a similar attenuation coefficient for field radiance at all three zenith angles.

The shape of the asymptotic radiance distribution was, however, different in the three investigated sediments. In the diatom sediment, which had the strongest extinction of light, the radiance distribution was dominated throughout the sediment by a strong component of downwelling and forward-scattered light at zenith angles close to 0° (Fig. 4F). In the wet quartz sand, the light field was much more diffuse, and already at 1-mm depth, downwelling light (zenith angles from 0° to 90°) had a nearly isotropic distribution (Fig. 4D). Downwelling light in dry quartz sand also exhibited a much more diffuse light field, although a totally isotropic distribution of downwelling light was not reached (Fig. 4B). Comparison of the upwelling radiances showed that the highest amount of backscattered light was found in dry quartz sand. In all sediments, the radiance distributions demonstrated a light field dominated by forward scattering of light (i.e. with highest values of field radiances at zenith angles from 0° to 90°).

Scalar irradiance—From the radiance distributions shown in Fig. 4, we calculated the depth distributions of scalar irradiance for 650-nm light (Fig. 5). At the surface of the sediment, the presence of an anisotropic light field composed of a strong directional component and a component of diffuse scattered light (*see Fig. 4*) resulted in a buildup of total light at the sediment surface, i.e. E_0 levels exceeding incident scalar irradiance (Fig. 5A). This effect was strongest in the highly scattering quartz sand, where scalar irradiance increased up to 175–180% of incident downwelling scalar irradiance at the sediment surface in dry sand and up to 135% of that in wet sand. Below a depth of 1 mm, scalar irradiance was attenuated exponentially with depth in the quartz sand. In the diatom sediment, with higher absorption due to the presence of microalgae, detritus, etc., scalar irradiance reached a maximum of only 105% relative to incident light at the sediment surface, and scalar irradiance decreased exponentially with depth from right below the sediment surface (Fig. 5A). Atten-

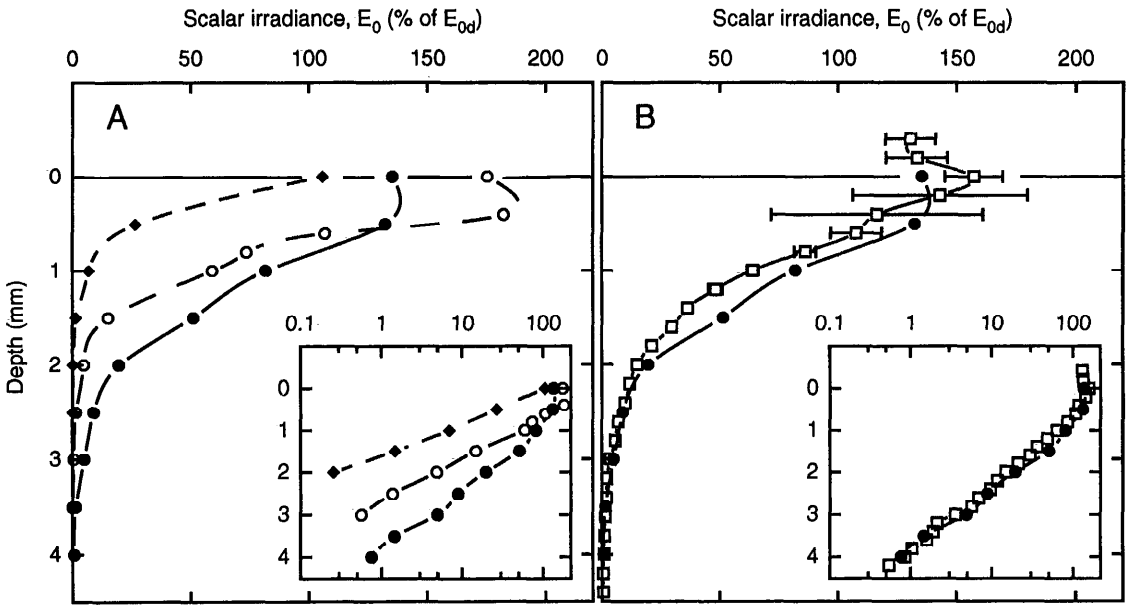

Fig. 5. Depth profiles of scalar irradiance, E_0, for 650-nm light in three types of sediment. A. Calculated scalar irradiances expressed as percent of incident downwelling scalar irradiance, E_{0d}. Dry sand—○; wet sand—●; coastal sediment with diatoms—◆. B. Comparison of scalar irradiances in wet sand, calculated (Fig. 4A—●) or measured directly by a scalar irradiance microsensor—□ (arithmetic mean of three measurements; error bars indicate SD). Inserts show depth profiles of logarithmically transformed data.

uation of scalar irradiance at 650 nm was highest in the diatom sediment, followed by dry and wet quartz sand (*see insert in Fig. 5A*).

Comparison of depth profiles of calculated scalar irradiance and directly measured scalar irradiance for 650-nm light in wet quartz sand showed a high degree of similarity with almost identical attenuation coefficients [K_{E_0} (calculated) = 1.68 mm^{-1}, K_{E_0} (measured) = 1.48 mm^{-1}] (Fig. 5B). However, close to the sediment surface the directly measured scalar irradiance values were higher than calculated values and reached a maximum at 157% of incident irradiance.

The spectral depth distribution of calculated scalar irradiance exhibited no sharp spectral signals in wet quartz sand, where light attenuation increased gradually from the infrared (IR) to the blue part of the spectrum (Fig. 6A). In the diatom sediment, light at 450–550 nm was attenuated much more than IR light, and a distinct trough at 675 nm corresponded with the absorption maximum of Chl *a* in the microalgae (Fig. 6B). Maximum values of scalar irradiance also varied with wavelength in both sediments and reached highest values for IR light of around 180% of incident irradiance in wet quartz sand and 120% in the diatom sediment.

Up- and downwelling irradiance and scalar irradiance—Radiance data were used to calculate the depth distribution of up- and downwelling irradiance and scalar irradiance (Fig. 7). The maximum of scalar irradiance, E_0 in the upper 0.0–0.5 mm of the quartz sand (Fig. 6), was caused by a combination of a high upwelling scalar irradiance component, E_{0u}, and a more or less constant downwelling component of scalar irradiance, E_{0_d} (Fig. 7A,C). In the dry quartz sand, upwelling scalar irradiance at the sediment surface was almost as high as downwelling scalar irradiance. Downwelling scalar irradiance increased to a maximum at 0.5-mm depth and then decreased exponentially with depth, while upwelling scalar irradiance decreased exponentially with depth from right below the sediment surface (Fig. 7A). In the wet quartz sand, upwelling scalar irradiance was <50% of downwelling scalar irradiance at the sediment surface. Both parameters were almost constant in the upper 0.5 mm of the wet quartz sand and then decreased

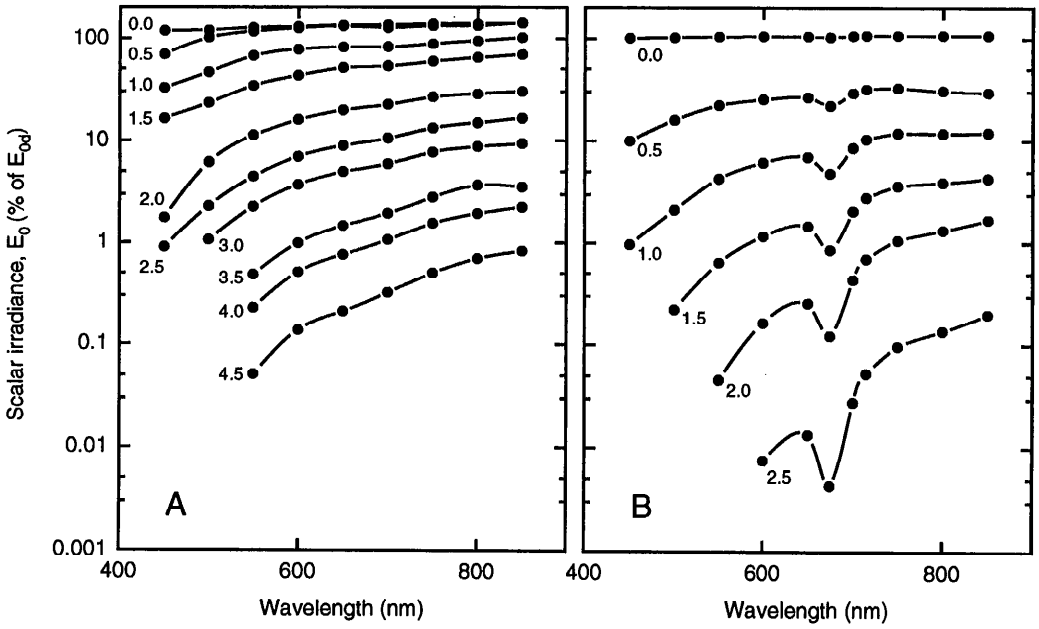

Fig. 6. Spectra of scalar irradiance, E_0, in two sediment types. A. Wet sand (125–250-μm particle size). B. Coastal sediment with diatoms. Numbers on curves indicate depth below the sediment surface. Data were normalized to incident downwelling scalar irradiance at the sediment surface and are presented on a logarithmic scale.

exponentially with depth (Fig. 7C). The steep decrease of scalar irradiance right from the surface in the coastal sediment with diatoms was due to much less upwelling light in the upper sediment layers (<10% of E_{0d}) (Fig. 7E).

E_d and E_u exhibited a similar depth distribution, but their values were lower than the corresponding downwelling and upwelling scalar irradiance values in the sediments (Fig. 7B,D,F). Both upwelling and downwelling components of scalar irradiance and irradiance were attenuated exponentially with depth below 0.5–1 mm from the sediment surface, and the log-linear and parallel depth profiles confirm the (asymptotic) attenuation coefficient found for field radiance (Table 2).

Average cosines and irradiance reflectance—From the depth distribution of scalar irradiance and irradiance components (Fig. 7), we determined the changes with depth of the angular light field by calculating average cosines and irradiance reflectance for 650-nm light (Fig. 8; Table 2). The average cosines exhibited large changes in the upper millimeter of the sediment and then approached an asymptotic value in deeper sediment layers, reflecting the transition from an anisotropic light field at the sediment surface to an asymptotic radiance distribution in the deeper sediment layers (Fig. 8).

Asymptotic values of average cosines (μ_a) for 650-nm light are given in Table 2. The average cosine, μ, increased with depth in the upper millimeter of the dry quartz sand (Fig. 8A), whereas it decreased strongly over the upper millimeter of both wet quartz sand and the diatom sediment (Fig. 8C,E). Average cosine at the sediment surface was higher in the diatom sediment ($\mu \sim 0.9$) than in wet quartz sand ($\mu \sim 0.6$) due to a much lower contribution of scattered light to the total light field at the surface of the diatom sediment (*see Fig. 4E*).

At the surface of all sediments, the downwelling light field was strongly dominated by incident collimated light, and values of μ_d varied from 0.9 in quartz sand to 0.98 in the diatom sediment (Fig. 8B,D,F). Below the sediment surface, the downwelling average cosine approached an asymptotic value, μ_{da} (Table 2). At depths below 1 mm in the wet quartz sand, μ_d was close to the theoretical value for an isotropic angular distribution of downwelling light ($\mu_d = 0.5$). μ_u was close to 0.5 at the surface

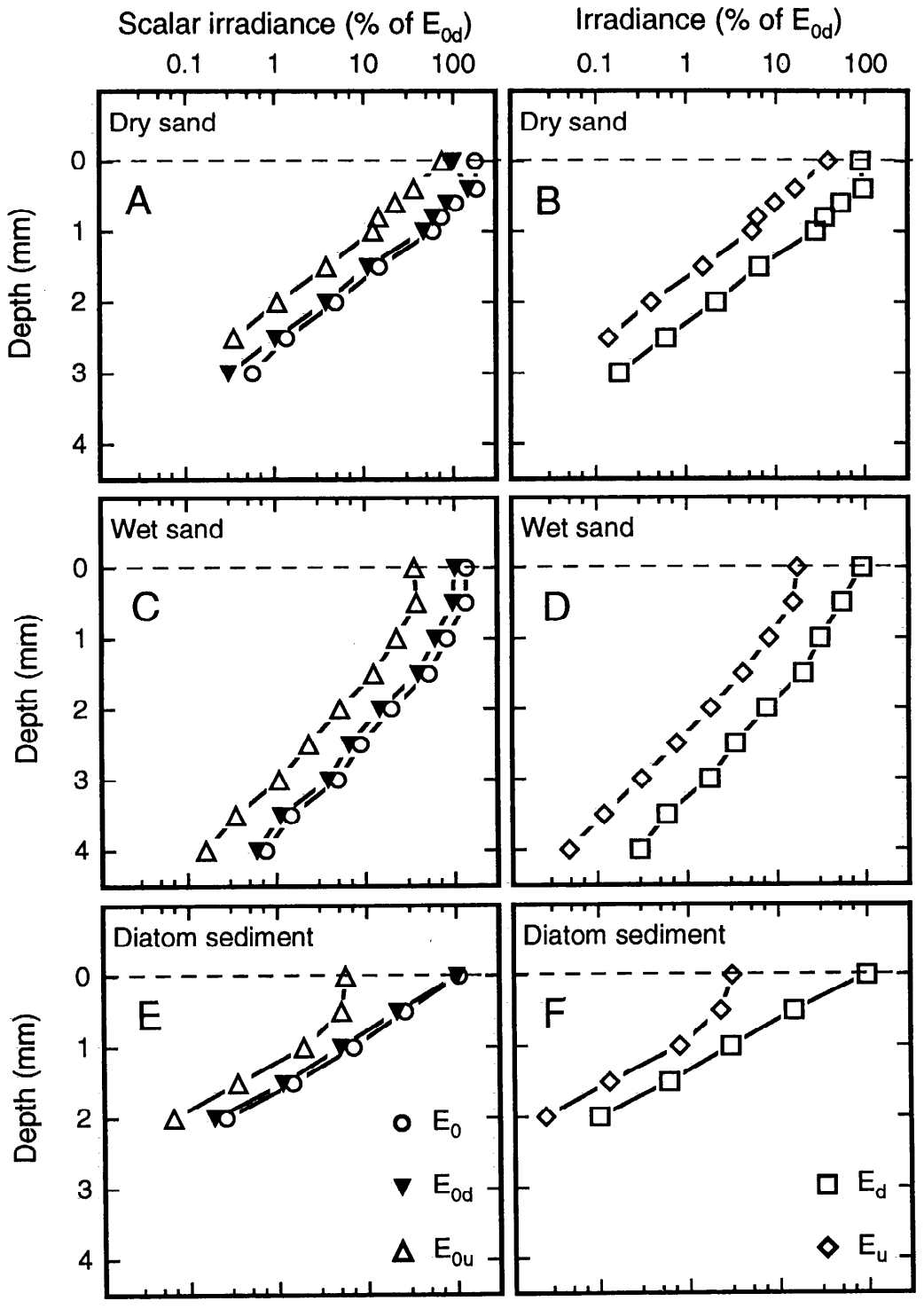
Scalar irradiance (% of E_{0d})
0.1
1
10
100
Irradiance (% of E_{0d})
0.1
1
10
100
Depth (mm)
0
1
2
3
4
Dry sand
A
Dry sand
B
Wet sand
C
Wet sand
D
Diatom sediment
E
Diatom sediment
F
E_0
E_{0d}
E_{0u}
E_d
E_u

of all investigated sediments, indicating that backscattered light from the sediment surface had an almost isotropic angular distribution. Below the sediment surface, μ_u decreased, indicating a less isotropic distribution of upwelling light.

Irradiance reflectance, R, was highest at the surface of dry quartz sand (Fig. 8A) where it reached a value of 0.42 (equivalent to 42% of incident irradiance) and then decreased to an asymptotic value of 0.2 in the sediment. At the surface of wet quartz sand, irradiance reflectance was only 0.18, while the asymptotic value was the same as in dry sand (Fig. 8B). At the surface of the diatom sediment, we observed a much lower irradiance reflectance (R = 0.03) which then increased over the upper 0–1 mm to an asymptotic value of R = 0.25 (Fig. 8C).

Spectra of asymptotic values for average cosines and irradiance reflectance calculated for wet quartz sand and the diatom sediment are shown in Fig. 9. Although the shape of the asymptotic radiance distribution differed (Fig. 4), spectra of μ_a in wet quartz and in diatom sediment showed identical values throughout much of the visible spectrum except at 450 and 675 nm, where μ_a reached maximal values in the diatom sediment (Fig. 9A). Average cosine of IR light was lowest in the diatom sediment.

Spectra of asymptotic downwelling average cosine revealed almost identical values of μ_{da} for IR light in both sediments, whereas downwelling average cosine for visible light was higher in the diatom sediment, with a slight maximum at 675 nm (Fig. 9B). Downwelling average cosines were always higher than the corresponding upwelling average cosines, indicating a downwelling light field in both sediments which was more forward directed than the upwelling light field. Whereas the diatom sediment exhibited the highest values of μ_{da} and μ_{ua} at shorter wavelengths, the opposite was observed in the quartz sand, where values were highest in the IR part of the spectrum.

Table 2. Asymptotic values of optical parameters and absorption coefficients for 650-nm light in two types of sediment.

Sediment type		Attenuation coefficient (mm^{-1})*												
		K_r†	K_{od}	K_{ou}	K_o	K_d	K_u	K_E	K_a	μ_{da}	μ_{ua}	μ_a	R_a	a
Sand, 125–250 μm														
Dry	x	2.32	2.36	2.23	2.33	2.40	2.28	2.43	2.33	0.60	0.41	0.37	0.20	0.86
	(±SD)	(±0.18)							(±0.19)	(±0.03)	(±0.02)	(±0.03)	(±0.03)	(±0.10)
Wet	x	1.75	1.66	1.75	1.68	1.68	1.79	1.65	1.73	0.51	0.33	0.31	0.20	0.54
	(±SD)	(±0.12)							(±0.13)	(±0.03)	(±0.02)	(±0.02)	(±0.03)	(±0.05)
Coastal sediment														
Wet	x	3.42	3.28	3.39	3.31	3.36	3.47	3.33	3.39	0.55	0.39	0.31	0.25	1.05
	(±SD)	(±0.24)							(±0.25)	(±0.03)	(±0.02)	(±0.01)	(±0.03)	(±0.12)

* Attenuation coefficients calculated from the log-linear part of depth profiles below 1 mm from the sediment surface (r^2 > 0.98–0.99).
† Mean of radiance depth profiles at zenith angle 0°, 20°, 40°, 60°, 80°, 100°, 120°, 140°, 160°, and 180°.

Fig. 7. Depth profiles of scalar irradiance and irradiance at 650 nm calculated from field radiance distributions in the three types of sediment. All data were normalized to incident downwelling scalar irradiance at the sediment surface and are presented on a logarithmic scale.

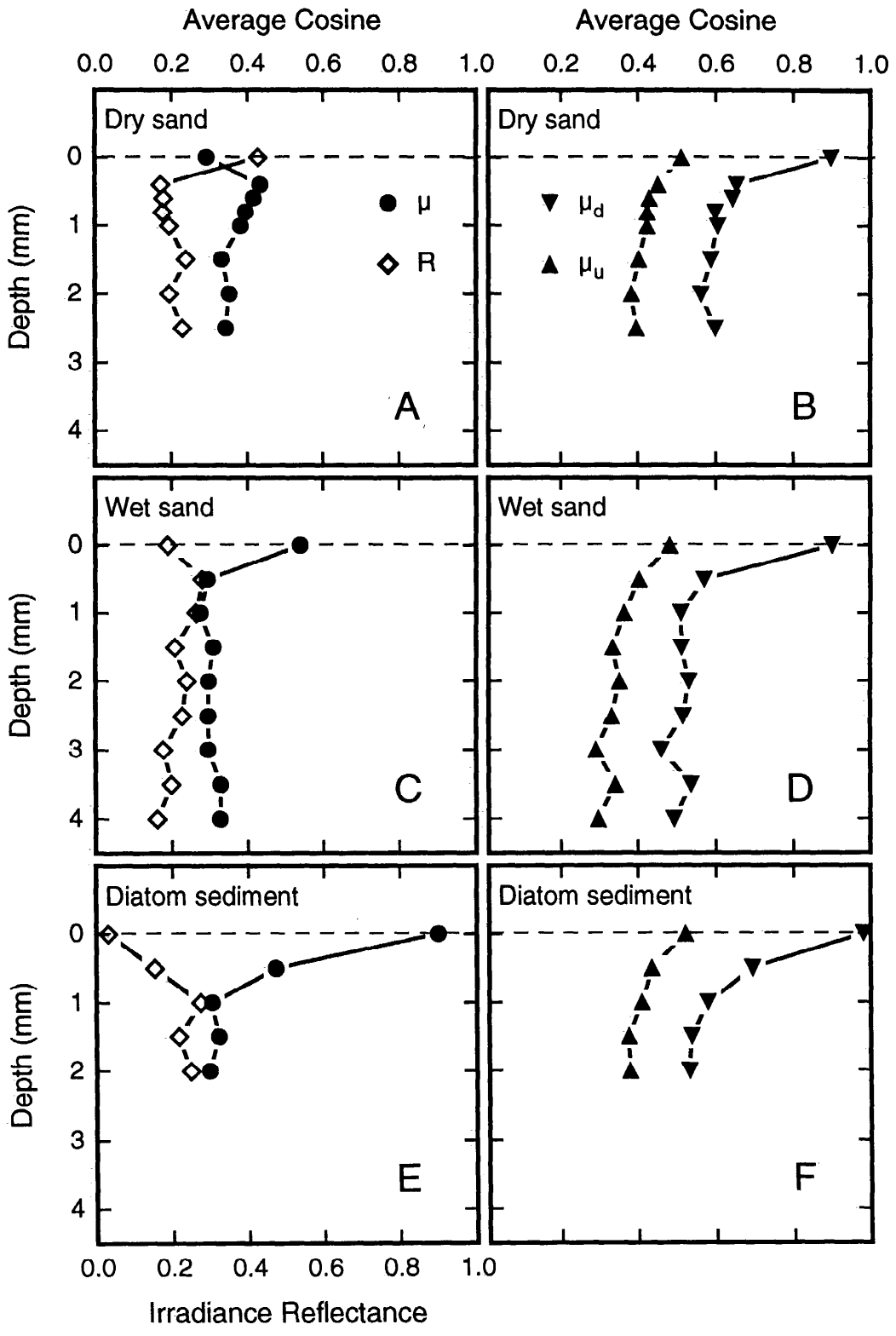
Average Cosine
0.0 0.2 0.4 0.6 0.8 1.0
Average Cosine
0.2 0.4 0.6 0.8 1.0
Dry sand
μ
R
A
Dry sand
μ_d
μ_u
B
Wet sand
C
Wet sand
D
Diatom sediment
E
Diatom sediment
F
Depth (mm)
0 1 2 3 4
Irradiance Reflectance

Spectra of asymptotic irradiance reflectance showed a higher reflectance in diatom sediment than in wet quartz sand throughout the spectrum (Fig. 9C), with minima at 450 and 675 nm where absorption was highest. Both sediments exhibited highest reflectance values for IR light.

Spectra of asymptotic attenuation coefficients and absorption coefficients—The light field approached an asymptotic state 1 mm below the sediment surface, showing an exponential attenuation of light with the asymptotic attenuation coefficient, K_a (Figs. 3, 6; Table 2). In the diatom sediment, K_a was highest in the blue-green (450–550 nm) region of the spectrum and at 675 nm, corresponding to the absorption maximum of Chl *a* in the diatoms (Fig. 10). Values of K_a ranged from 5 mm^{-1} for blue light at 450 nm to 2 mm^{-1} for IR light at 850 nm. Spectral attenuation coefficients were lower in wet quartz sand where no spectral signals from photopigments were found, and K_a thus decreased continuously from highest values in the blue part of the spectrum (2.2 mm^{-1}) to lowest values for IR light (1.5 mm^{-1}).

Spectral absorption coefficients were calculated from the asymptotic values of μ_a and K_a (Eq. 11, Fig. 10). In wet quartz sand and in diatom sediment, the absorption spectra demonstrated the same spectral features as the respective attenuation spectra, but values of absorption coefficients were much lower than the corresponding attenuation coefficients. The absorption coefficient, *a*, in wet quartz sand exhibited only a minor spectral variation, from 0.7 mm^{-1} at 450 nm to 0.4 mm^{-1} at 850 nm. In the diatom sediment, *a* ranged from 1.8 mm^{-1} at 450 nm to 0.5 mm^{-1} 850 nm, with a Chl *a* absorption maximum of 1.2 mm^{-1}at 675 nm.

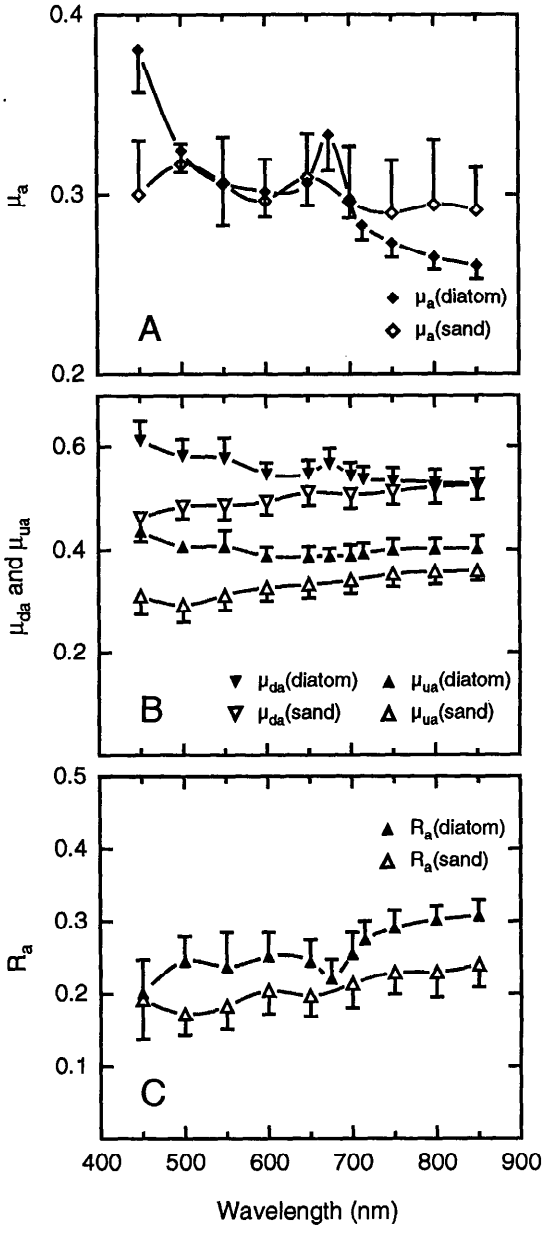

Fig. 9. Spectra of asymptotic values of average cosines and irradiance reflectance in wet sand (125–250-μm particle size) and coastal sediment with diatoms. A. Average cosine, μ_a. B. Downwelling, μ_{da}, and upwelling, μ_{ua}, average cosines. C. Irradiance reflectance, R_a.

Discussion

Components of the light field—When one interprets radiance measurements taken with fiber-optic microprobes, it is important to consider the experimental setup and how it affects the light field at different zenith angles and at

←

Fig. 8. Depth profiles of average cosines (μ, μ_d, and μ_u) and irradiance reflectance (R) for 650-nm light in the three types of sediments.

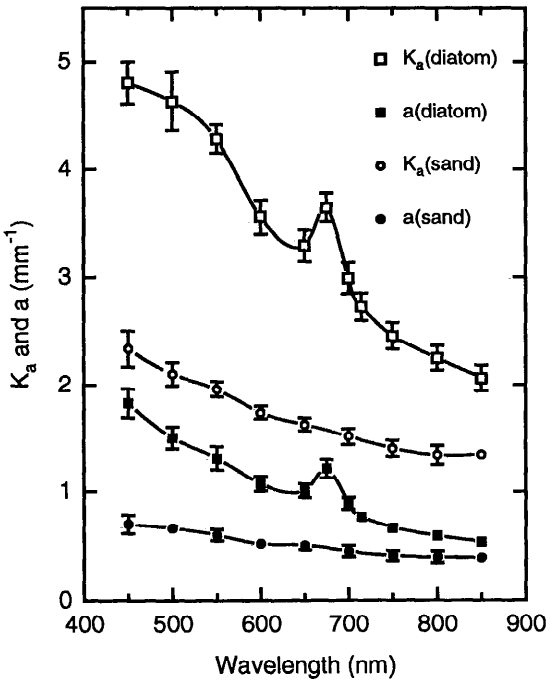

Fig. 10. Spectra of the asymptotic diffuse attenuation coefficient, K_a, and absorption coefficient, a, in wet sand (125–250-μm particle size) and coastal sediment with diatoms.

different depths in the sediment (Fig. 11). In our experiments at the sediment surface at 0° zenith angle, the radiance probe directly collected incident collimated light, which was the dominating component of the surface light field (Fig. 4). Just below the sediment surface, the large decrease in 0° radiance (Fig. 3) was due to intense scattering of collimated light out of the downwelling light path by the sediment particles, and the fiber probe thus collected a combination of downwelling and forward-scattered light at 0° zenith angle, which then became a less important part of the total amount of light (Fig. 4). The abrupt shift from a collimated to a diffuse light field was also evident from the subsurface maximum of forward-scattered light at 20°–60° zenith angles (Figs. 3, 4).

An important difference between dry and wet sediments was the contribution of forward-scattered light at the sediment surface of wet sediments caused by the presence of an overlying water layer (cf. Fig. 4A,C). As water has a higher refractive index than air, diffuse reflected light from the wet sediment surface could be redirected back to the sediment surface by reflection at the water–air interface (Fig.

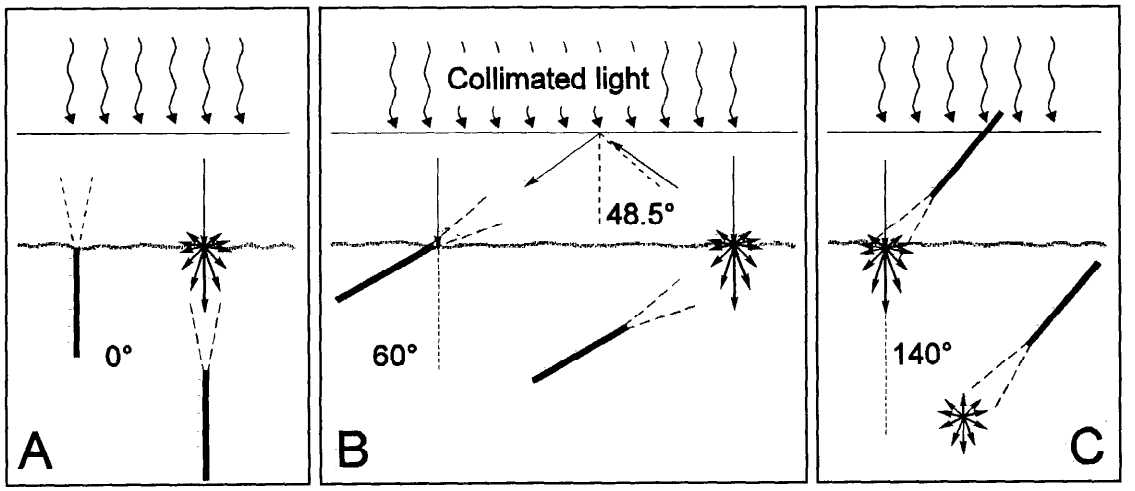

Fig. 11. Components of the light field measured by fiber-optic radiance probes at different zenith angles relative to the incident collimated light. A. At 0° the fiber probe mainly collects incident collimated light at the sediment surface. Below the surface the fiber collects downwelling light composed of both a directional and a forward-scattered component. B. At 20°–80° the fiber probe collects predominantly forward-scattered light. In the presence of a water film on top of the sediment, the fiber probe also collects diffuse downwelling light at the sediment surface originating from backscattered light from the sediment which has been internally reflected at the water–air interface. Above an incidence angle of 48.5°, total internal reflection of light occurs at the water–air interface. C. At zenith angles >90° the optical fiber probe collects backscattered light.

11B). Reflection at the water–air interface is determined by the relative refractive index of water to air (~1.33), which, according to Snell's law of refraction, leads to a critical angle of ~48.5° for total reflectance of incident light reflected from the sediment surface. Only a minor part of the light incident on the water–air interface at smaller angles than the critical angle will thus be reflected, whereas light incident at larger angles than the critical angle will undergo total internal reflection at the water–air interface and thus establish diffuse downwelling light at the sediment surface.

The contribution of this internally reflected light to the downwelling light at the sediment surface could be calculated as the ratio of downwelling scalar irradiance, E_{0d}, to the theoretical amount of incident collimated light in the absence of internal reflection, which is equivalent to the weighted downwelling radiance at 0° zenith angle, L_d (Fig. 12). We found the largest effect of internal reflection in wet quartz sand, where diffuse downwelling light resulted in 10–20% higher scalar irradiance at the sediment surface. In the diatom sediment, which had a much lower reflectance than wet quartz sand, internally reflected light only accounted for 2–3% more downwelling light at the sediment surface with a minimum at 675 nm, due to the presence of microalgae. Highest amounts of internally reflected light were found in the IR part of the spectrum in accordance with the measured reflectance spectra of the sediments (Fig. 9C). Also, for water-covered sediments in nature, such diffuse downwelling light must contribute to illumination, although the importance and distribution of double-reflected light is here affected by absorption during two passages through the water column and by wave motion of the reflecting water–air interface.

Upwelling radiance (Fig. 11C) exhibited an almost isotropic angular distribution at the sediment surface (Fig. 4). A surface exhibiting the same radiance at all zenith angles from 90° to 180° is called a Lambertian reflector, for which the upwelling irradiance, E_u, can be calculated from the upwelling radiance, L_u, as $E_u = \pi L_u$ (Kortüm 1969; Kirk 1983). The ratio $E_u : L_u$ (i.e. the inverse of the radiance reflectance) can thus be used as a measure for isotropy of the upwelling light field and would become equal to π for a perfectly isotropic upwelling light field. Values of $E_u : L_u$ for 650-nm light were very close to the theoretical value ($\pi = 3.14$) for an isotropic light field (dry sand, 3.22; wet sand, 3.29; diatom sediment, 3.20). Similar values were found throughout the spectral range investigated in wet quartz sand and in diatom sediment, which exhibited the most isotropic distribution of reflected light (Fig. 13). In optical oceanography, upwelling light in water is much less isotropic with $E_u : L_u$ values of ~5 (Kirk 1983). The isotropy of reflected light from the sediment surface is due to the combined effect of multiple scattering in many randomly oriented scattering particles which form an optically rough surface with diffuse backscattering and reflection. Accordingly, sand along the beach appears equally bright when observed at different angles.

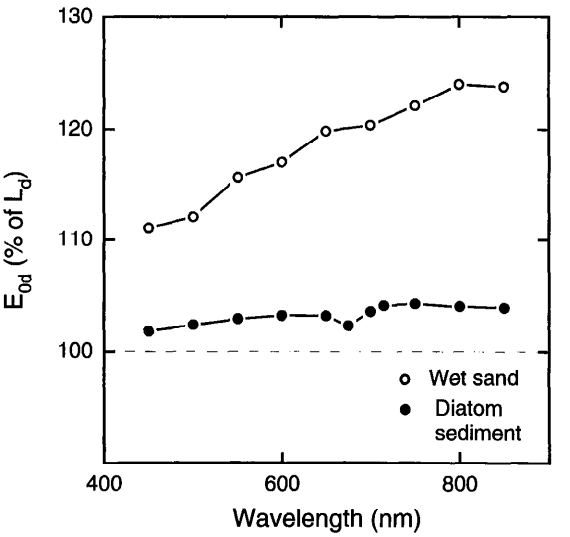

Fig. 12. Ratio of downwelling spectral scalar irradiance, E_{0d}, and the weighted downwelling radiance (0°) at the sediment surface, L_d, expressed in percent of L_d. The ratio quantifies the additional incident light at the sediment surface due to internal reflection at the water–air interface of diffuse backscattered light from the sediment. Dashed line indicates the ratio for a perfectly collimated incident light field in the absence of internal reflection.

Light propagation in dry and wet quartz sand—Light penetration was lower in dry quartz sand than in wet sand with an overlying water film of a few millimeters (Figs. 3–6). The asymptotic attenuation coefficient, K_a, was 2.34 mm^{-1} in dry sand and 1.70 mm^{-1} in wet sand for 650-nm light (Table 2). Similar results have been reported in the relatively few other stud-

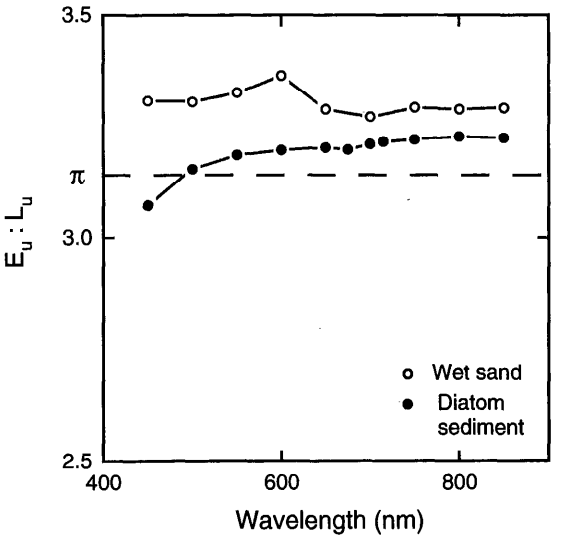

Fig. 13. Ratio of upwelling spectral irradiance, E_u, and average upwelling radiance, L_u, at the sediment surface used as a measure for isotropy of the light field. Dashed line indicates the value for a perfect isotropic distribution of upwelling light. L_u was calculated as the average of the upwelling radiance at 100°, 120°, 140°, 160°, and 180° zenith angle (relative SD was 5–20%).

ies of light penetration in sandy soils and sediments (Hoffmann 1949; Woolley and Stoller 1978; Bliss and Smith 1985; Tester and Morris 1987; Mandoli et al. 1990). An effect of wetting which can easily be observed on the beach is that the surface of wet sand appears darker than dry sand, i.e. the albedo (surface irradiance reflectance) is lower for wet than for dry sand (Ångström 1925; Sellers 1965; Bohren 1983). In our study, we observed a reflectance ~60% lower for 650-nm light from wet sand (R = 0.18) than from dry sand (R = 0.42). Both the higher transmission and the lower reflection of light in wet vs. dry sediment are due to the smaller difference between the refractive index of quartz sand (n ~ 1.5; cf. Twomey et al. 1986) and water (n_0 ~ 1.33), than the difference between quartz sand and air (n_0 ~ 1) (Hoffmann 1949; Fenchel and Straarup 1971). The particle size of the sand is much larger than the wavelength of light and thus approaches a scattering efficiency which is independent of size and refractive index of the particles (*see theory and calculations*). Thus, the observed changes cannot be due to a simple decrease in optical effective size of the sediment particles (resulting in a lower scattering efficiency) when the refractive index of the surrounding medium approaches the particle refractive index.

A simple model for the physical mechanism causing the observed darkening of rough sediment surfaces upon wetting was proposed by Ångström (1925) based on the effect of the water film covering the wet sediment. The rough sand surface leads to diffuse reflection of light, which, for large angles of incidence, can be totally internally reflected at the water–air interface. Diffuse reflected light from the sediment can thus be redirected by internal reflection in the water–air interface into the sediment, resulting in a higher probability of absorption in the surface layer, which then appears darker. Ångström's model was recently reformulated and extended by Lekner and Dorf (1988), who showed that the darkening effect will be strongest for sediments with low absorption. High absorption leads to a higher probability that incident light will be absorbed on the first interaction with the sediment surface, resulting in much less light scattering and thus less light redirected into the sediment by the water film.

An alternative model was formulated by Bohren (1983) and Twomey et al. (1986), who explained the darkening as the combined effect of multiple scattering and a change in the angular distribution of light scattered by single particles upon wetting of the sediment. The closer the refractive index of the surrounding medium matches the particle refractive index, the smaller the scattering angle (Bohren 1983). Wetting of dry quartz sand thus results in a more forwardly directed angular distribution of light from single-event particle scattering. The average cosine of scattering angle, μ_s, thus comes closer to 1 in wet sand, equivalent to an average scattering angle closer to 0°. A smaller particle scattering angle affects the reflectance of a sediment because photons have to undergo more scattering events before reemerging at the sediment surface. The shortest possible path for an incident photon before reemerging thus becomes longer as the scattering angle becomes smaller (Bohren 1983). For each encounter with a particle there is a certain probability of absorption. Increasing the number of scattering events thus increases the probability of absorption of upwelling photons on their way to the sediment surface, and the

surface therefore appears darker. As in the model of Ångström (1925), the darkening effect will be strongest in sediments with a high scattering to absorption ratio (i.e. a high particle-scattering albedo, ω_0, as is the case in quartz sand, $\omega_0 > 0.9$). A lower scattering albedo and thus a higher absorption $(1 - \omega_0)$ would make multiple scattering effects less distinct because much of the light would be absorbed within the first few scattering events irrespective of the scattering angle, thus making an increase in optical pathlength for upwelling photons less important for the observed attenuation of light.

Our results for 650-nm light in dry and wet quartz sand show that both described mechanisms are important for change in the near-surface light field of sandy sediments. This is the first time the two models have been verified by direct measurements of the light field. The water film on top of the wet quartz sand resulted in a surface light field with significant amounts (~20% of collimated incident light at 650 nm) of downwelling diffuse light at zenith angles >40° originating from backscattered light from the water–air interface (Figs. 3B, 4C, 12).

We did not compare dry and wet coastal sediments with higher absorption. Our results from the diatom sediment did, however, confirm the conclusion of Lekner and Dorf (1988) that the amount of light internally reflected at the water–air interface is lower (only ~3% of incident collimated light in the diatom sediment, Figs. 4E, 12) for sediments with relatively high absorption and low reflectance. Assuming a near isotropic distribution of reflected light from the sediment surface (as was the case in all our measurements, *see Figs. 4, 13*), Ångström (1925) calculated a theoretical decrease in the reflectance of ~60% upon wetting of a dry sediment. Almost the same value was predicted by the extended models of Lekner and Dorf (1988) and Twomey et al. (1986). We observed a 57% lower reflectance in wet quartz sand than in dry sand.

A geometrical mechanism of internal reflection at the air–water interface is confirmed by our data for irradiance reflectance and the angular radiance distribution of the downwelling light field at the sediment surface. However, the mechanism of internal reflection is of quantitative importance only for the surface light field of sediments covered with a few millimeters of water and cannot account for the higher light penetration and other differences between the light field in wet vs. dry sand.

The observed angular light field in wet sand was more forward biased than in dry sand, which had relatively more backscattered light (Fig. 4). While the single scattering albedo is unchanged by wetting, wet sand exhibits a smaller average particle scattering angle than dry sand, primarily due to a more forward-directed scattering of refracted and reflected light (Twomey et al. 1986). Consequently, we detected more forward-scattered light at zenith angles >20° in wet sand, leading to more downwelling photons and, thus, higher light penetration (cf. Fig. 4B,D). Because of the smaller average scattering angle, upwelling photons needed more scattering events before re-emerging at the sediment surface and they were therefore subject to a higher probability of absorption than in dry sand, leading to fewer upwelling photons and a lower surface irradiance reflectance in wet sand. This mechanism also accounts for the general observation that the upwelling average cosine decreases below the sediment surface (Fig. 8), leading to a less isotropic distribution of upwelling light in the sediment, which was most pronounced in wet quartz sand (Fig. 4).

In dry sand, the average cosine and irradiance reflectance exhibit a strange behavior near the sediment surface (Fig. 8A). Here μ was 0.3 at the sediment surface despite the downwelling average cosine being >0.9 and the upwelling average cosine being close to 0.5. It is possible, however, to derive the average cosine from the up- and downwelling average cosine and the irradiance reflectance (J. T. O. Kirk pers. comm.).

By definition

$$E_0 = E_{0d} + E_{0u} = \frac{E_d}{\mu_d} + \frac{E_u}{\mu_u} = \frac{\mu_u E_d + \mu_d E_u}{\mu_d \mu_u}. \quad (13)$$

Thus

$$\mu = \frac{E_d - E_u}{E_0} = \mu_d \mu_u \frac{(E_d - E_u)}{(\mu_u E_d + \mu_d E_u)}, \quad (14)$$

which can be rearranged to

$$\mu = \mu_d \mu_u \left[\frac{1}{\mu_u + (\mu_d R)} - \frac{1}{\mu_d + (\mu_u / R)} \right]. \quad (15)$$

For all three sediments, the average cosine calculated from Eq. 15 was identical to the average cosine calculated from the radiance distribution. The most important factor determining the average cosine in the different sediments is the irradiance reflectance, R. The decrease of R below the surface in the dry sand thus explains the observed increase of μ. The mechanism behind the decrease of R is not yet clear, but it could be due simply to an error caused by the heterogeneity of the particle distribution and especially to the packaging of the sand grains, which was less defined in the dry sediment.

Light propagation in coastal sediment with microalgae—The light field in the diatom sediment exhibited a strongly forward-peaked radiance distribution throughout the sediment with much less scattered light than in sand (Fig. 4). For a purely isotropically scattering and nonabsorbing medium, the radiance distribution is isotropic, while for anisotropically scattering media or media exhibiting both scattering and absorption, the radiance distribution becomes forward biased (Timofeeva 1974). In the latter case, photons travelling at oblique angles exhibit a longer pathlength per unit of vertical distance traversed, thereby increasing their probability of being absorbed or redirected into the upwelling light stream as compared to photons travelling in a more forward direction (Kirk 1991). This effect is more pronounced the higher the absorption coefficient. Thus, the persistence of a forward-peaked angular radiance distribution with depth in the diatom sediment was due to a more effective removal of obliquely travelling photons by absorption.

Importance of particle size and wavelength—All sediments exhibited highest penetration of IR light, while blue light was most strongly attenuated (Fig. 6). Multiple scattering of light by large particles enhances light penetration at wavelengths subject to low absorption. Thus, despite a short mean free path between photon–particle interactions due to a high attenuation coefficient, for IR light, most of these interactions are scattering events rather than absorption events. At the same time, the single scattering distribution is highly forward directed, so IR photons continue to penetrate into the sediment even after multiple scattering events (Wilson and Jaques 1990).

Spectral variation was most pronounced in the diatom sediment, which had much higher attenuation and absorption coefficients than quartz sand (Fig. 10). Similar spectra and values of attenuation coefficients were found by Haardt and Nielsen (1980) in coastal sediments with microalgae and by Fenchel and Straarup (1971) in rinsed quartz sand. Both studies also demonstrated increasing attenuation coefficients with decreasing particle size or with increasing amounts of organic matter in the sediments. Compared to attenuation and absorption coefficients of natural waters, which range from <0.01 m^{-1} in the clearest oceanic waters to >10 m^{-1} in extremely turbid lakes (Kirk 1983), attenuation of light in the investigated sediments was 10^2–10^5-fold higher.

Besides the high absorption by photosynthetic pigments and amorphous organic matter, scattering may also play an important role in the observed attenuation spectra in the diatom sediment. For particle sizes less than or comparable to the wavelength of light, particle scattering is strongly dependent on wavelength, λ, exhibiting inverse proportionality between the scattering coefficient and λ^2–λ^4 (Kortüm 1969). For large particles, scattering becomes approximately inversely proportional to λ. The diatom sediment in our study was composed of a mixture of relatively large sand grains (>50 μm), microalgae ($\sim$1–50 μm), and organic material, with small particle sizes ranging from <1 μm up to $\sim$50 μm. The organic material, especially, could thus contribute to a higher spectral variation of attenuation due to scattering. The quartz sand was composed of relatively large particles, ranging from 125 to 250 μm in size and with a low absorption; consequently, the attenuation of light in quartz sand exhibited a much lower spectral variation. A detailed study of light penetration in sediments of different particle sizes is presented elsewhere (Kühl et al. 1994*a*).

Spectra of average cosines—The spectral variation of attenuation and absorption also affected the angular distribution of light as characterized by the asymptotic values of the

three average cosines (Fig. 9A,B). The average cosine, μ_a, revealed only small differences between quartz sand and diatom sediment, although the angular light distribution differed significantly (Figs. 4, 9A). The average cosine is an integral measure of the cosine of the mean angle of light propagation for both up- and downwelling photons (*see notation for light field parameters*). Different angular light fields can thus exhibit the same average cosine as long as the integrated amount of up- and downwelling photons travelling at different zenith angles is the same. Higher values of average cosine for blue light and light at 675 nm in the diatom sediment indicated, however, a more directional light field because of the correspondingly higher absorption at these wavelengths (Fig. 9A). At the same time, average cosine was lower for IR light in the diatom sediment than in quartz sand, indicating a relatively more isotropic distribution of scattered light because of a higher density of small particles in the diatom sediment.

Downwelling visible light was much more forward directed in the diatom sediment (indicated by a higher downwelling average cosine) than in quartz sand (Fig. 9B). The largest difference was found at wavelengths where absorption was highest. For IR light, the downwelling average cosine was identical in the two sediments and approached the theoretical value of 0.5 for a perfectly isotropic distribution. Upwelling light was closest to an isotropic distribution in the diatom sediment at all wavelengths as compared to quartz sand due to the higher density of small particles in the diatom sediment.

Scalar irradiance maximum—We observed a maximum of scalar irradiance in the upper 0.0–0.5 mm of the quartz sand (Figs. 5, 6), where it reached ~200% of incident irradiance in the IR part of the spectrum. The scalar irradiance maximum was lower in the diatom sediment, ~120% of incident light. In both sediments the scalar irradiance maxima closely followed the reflectance spectra, which also exhibited the highest reflectance for IR light (Fig. 9C).

Similar maxima of scalar irradiance in microbenthic communities were found in dense microbial mats and laminated coastal sediments (Jørgensen and Des Marais 1988; Lassen et al. 1992*b*; Kühl and Jørgensen 1992). The high density of phototrophic microorganisms in these systems resulted in a strong spectral variation of the maximal scalar irradiance values, with distinct minima at the absorption wavelengths of major photopigments. In dense cyanobacterial mats, a subsurface maximum for IR light of 200% of incident irradiance was observed at 0.1–0.2 mm below the surface, while visible light reached a maximum of 105–130% at the mat surface (Jørgensen and Des Marais 1988; Lassen et al. 1992*b*).

In mats with loose and gelatinous surface layers of diatoms, visible light also exhibited a subsurface maximum, reaching up to 180% of incident irradiance. Measurements in loose microbial mats with sand grains and in sandy coastal sediments always exhibited a surface maximum of scalar irradiance reaching 120–180% of incident irradiance for visible light and ~200% for IR light (Lassen et al. 1992*a,b*; Kühl and Jørgensen 1992; Figs. 5, 6). In studies of light penetration in plant and animal tissue, even higher maxima of scalar irradiance have been reported. Based on multidirectional radiance measurements, Vogelmann and Björn (1984) calculated a scalar irradiance maximum of 290% of incident irradiance for IR light inside a plant leaf. The most extreme values were measured in animal tissue and in phantom media of a known composition, where scalar irradiance maxima >300–400% of incident irradiance were found for visible light around 630 nm (Star et al. 1987; Profio 1989; Moes et al. 1989).

The observation of light maxima in the upper layers of sediments, microbial mats, and other turbid media exceeding the light incident on their surfaces may appear to be a violation of the laws of thermodynamics. Traditionally, light propagation is described by a simple exponential attenuation with depth according to Lambert-Beers law. However, this description is not valid in scattering media. According to the equation of radiative transfer (Eq. 9), there is a possibility for increase in radiant flux along a certain light path if the scattering of light into the light path is larger than the attenuation over the distance traversed. Such an increase of radiance with depth was observed over the upper 0.5 mm of the investigated sediments for forward-scattered light at zenith angles from

20° to 80° (Figs. 3, 4). Depending on the actual radiance distribution, integral measures of the light intensity (i.e. irradiance and scalar irradiance) can therefore also exhibit a near-surface maximum.

Multiple scattering increases the pathlength of photons per vertical distance traversed. Because photons have very high but fixed velocities in a medium, the increased pathlength caused by multiple scattering is equivalent to a longer residence time of photons within a certain sediment layer, thus leading to a higher flux density of photons close to the boundary, where light is continuously incident (*see* Anisimov and Fukshansky 1992; Fukshansky et al. 1993). The phenomenon can thus be explained in terms of rather simple physical mechanisms such as reflectance and refraction of light (e.g. Kaufmann and Hartmann 1988; Anderson et al. 1989).

Importance of backscattered light—In a nonscattering absorbing medium, total light at the surface equals the incident collimated light (i.e. scalar irradiance, E_0, is equal to the downwelling scalar irradiance, E_{0d}). In a turbid medium (such as a sediment), the total light intensity at the sediment surface, E_0, is the sum of incident collimated light, E_{0d}, plus a contribution from diffuse backscattered light, quantified by the diffuse reflectance, R. Our results demonstrate that backscattered light is almost perfectly isotropic near the sediment surface (Figs. 4, 13). For an isotropic distribution of backscattered light, the average pathlength for upwelling photons is exactly twice that of photons in a collimated beam traversing a thin plane of sediment (Kortüm 1969). The contribution of backscattered light at the sediment surface is therefore $2E_{0d}R$, and the total light intensity is thus given as

$$E_0(z_0) = E_{0d}(z_0)[1+2R(z_0)]. \quad (16)$$

Equation 16 holds for sediments where there is no optical boundary at the sediment surface caused by a difference in refractive index between the sediment and the surrounding medium. This is the case in sandy sediments such as the ones we investigated where sediment particles are surrounded by the same medium as above the sediment (i.e. air or water). We used Eq. 16 and the measured irradiance reflectance values for 650-nm light to calculate a theoretical surface maximum of scalar irradiance of 184 and 136% of incident irradiance in dry and wet quartz sand. The values calculated from measured radiance distributions were 175–180% in dry sand and 135–140% in wet sand. Thus, the higher reflectance of dry sand could account for the observed higher surface maximum of scalar irradiance of dry sand as compared to wet sand. For the diatom sediment, the theoretical value for the surface scalar irradiance at 650 nm was 110% of incident irradiance compared to the measured value of 106%. The theoretical model leading to Eq. 16 could thus closely describe the measured surface maximum in the investigated sediments.

Importance of refractive index—In microbial mats and biofilms with a high density of phototrophic microalgae and bacteria, high amounts of polysaccharides and other polymeric compounds are produced, forming a dense gelatinous matrix of exopolymers and microorganisms. If the refractive index of such a matrix is higher than the refractive index of the surrounding air or water, an optical boundary for upwelling photons is created at the interface between the microbial mat and the overlaying air or water. A shift in refractive index results in internal reflection of diffuse upwelling light at the optical boundary that redirects photons back into the microbial mat where they, together with the already mentioned diffuse upwelling light, contribute to the measured scalar irradiance near the surface. The significance of internal reflection depends on the difference in refractive index between the microbial mat and the surrounding medium, and the internal reflectance of diffuse light at the optical boundary, r, can be calculated by integration of Fresnel's equation (Anderson et al. 1989; Lekner and Dorf 1988). It can be shown (cf. Anderson et al. 1989) that the near-surface scalar irradiance in a medium exhibiting a refraction index mismatch with the surrounding medium can be calculated as

$$E_0 = E_{0d}\left[1 + 2R\frac{(1+r)}{(1-r)}\right]. \quad (17)$$

The ratio, $(1+r):(1-r)$, is always >1, and for refractive indices ranging from 1.3 to 1.6 relative to air, the ratio reaches values from 5 to >9 (Anderson et al. 1989). Thus even

maxima of scalar irradiance >400% of incident light can be expected, according to this model. Refractive index is thus a key parameter for the near-surface scalar irradiance in microbial mats and biofilms. To our knowledge, no measurements of refractive index have yet been done in microbial mats or biofilms in relation to measurements of scalar irradiance. As pointed out by Wilson and Jaques (1990) for biological tissues, such measurements are difficult due to a varying water content in the matrix of exopolymers and microorganisms.

The presence of an optical boundary makes the surface layer of microbial mats and biofilms act as a light trap. In these microbenthic communities, the importance of both the internal reflection term and the reflectance term in Eq. 17 depends heavily on wavelength due to the high density of photopigments. Given a scattering efficiency which is more or less independent of wavelength (due to the large particle size), photons at wavelengths which are absorbed strongly would exhibit a higher attenuation coefficient, c, and consequently a shorter mean free path, $1/c$, and a lower reflectance, R, than photons at wavelengths where scattering predominates absorption. The effects of backscattering and internal reflection would thus decrease, and at the same time, the scalar irradiance maximum for photons at wavelengths subject to high absorption would occur closer to the surface. At wavelengths where scattering predominates, the subsurface scalar irradiance maximum would reach higher values. The depth at which this subsurface maximum is observed would depend, however, on the mean free path of the photons, the shape of the scattering function (i.e. the average cosine of scattering angle, μ_s), and the scattering efficiency (i.e. the single scattering albedo, ω_0, Motamedi et al. 1989).

Thus, the simultaneous observation of a subsurface IR light maximum, a lower surface visible light maximum in dense microbial mats (Jørgensen and Des Marais 1988; Lassen et al. 1992*b*), and the subsurface visible light maximum in gelatinous mats with a lower light attenuation (Jørgensen and Des Marais 1988) can be attributed to the optical effects described above, because visible light exhibits a much higher extinction than IR light in these microbenthic communities. Evaluation of the proposed model and detailed discussion of the scalar irradiance maximum in dense laminated microbenthic communities (such as microbial mats), however, require measurements of the light field parameters with fiber-optic microprobes combined with independent measurements of the inherent optical parameters.

Calculated vs. measured scalar irradiance—Although the depth profiles of directly measured and calculated scalar irradiance in wet quartz sand were similar and exhibited almost the same attenuation coefficient in the deeper sediment layers, the measured surface maximum of scalar irradiance was higher than the calculated one (Fig. 5B). The observed difference was probably due to the lower spatial resolution and higher degree of variability of the radiance measurements. The small size of the scalar irradiance microprobe (~80 μm) enabled reproducible measurements at 0.2-mm spatial resolution, while radiance measurements were done only at 0.5-mm spatial resolution. A higher light intensity in the directly measured data could, however, also be due to locally increased scattering around the small diffusing sphere on the light-collecting end of the scalar irradiance microprobe. The importance of this effect is difficult to quantify, but comparison with the calculated scalar irradiance indicates that the effect in sand is much smaller than the observed surface maximum of scalar irradiance which therefore cannot be attributed to an artifact of the measuring technique. It is important, however, to keep in mind this interaction between the scalar irradiance fiber probe and its surroundings. A quantification and correction of such an effect will require detailed studies of combined radiance and scalar irradiance measurements in media with known composition and optical properties.

Asymptotic light field—While the light field in the upper sediment layers was affected by optical phenomena related to near-surface effects such as internal reflectance and diffuse backscattering, the angular light distribution in deeper sediment layers (>1 mm) became independent of depth and approached a constant angular radiance distribution (Fig. 4). Consequently, the attenuation coefficients of field radiance became independent of zenith angle and depth (Fig. 3) and exhibited the same attenuation coefficient as irradiance and scalar

irradiance (Fig. 7; Table 2). Furthermore, average cosines and irradiance reflectance approached asymptotic values as they became independent of depth in the sediment (Fig. 8; Table 2). A light field exhibiting the abovementioned characteristics is known as the asymptotic light field (IAPSO 1985); it is approached in homogeneous media at depths where the angular light distribution becomes independent of the incident light field and therefore is determined exclusively by the inherent absorption and scattering characteristics of the medium.

The existence of such an asymptotic light field in homogeneous aquatic media was shown theoretically by Preisendorfer (1959) and has been experimentally verified in several studies of radiance distribution in natural water masses (e.g. Tyler 1960) and in laboratory studies of turbid aqueous suspensions with different scattering and absorption properties (e.g. Herman and Lenoble 1964; Timofeeva 1974). The changes in the angular radiance distribution with depth reported for wet quartz sand in this study are similar to the results of Timofeeva (1974). The transition from an anisotropic angular light field to an asymptotic light regime reported by Timofeeva occurred, however, more gradually and reached the asymptotic state at greater depths due to a lower density and different scattering properties of the particles in the milky medium used. The present study is, to our knowledge, the first demonstration of an asymptotic light field in natural sediments.

Experimental difficulties and sources of error—We have not attempted a rigorous statistical analysis of our data because it would require substantially more data to quantify the different sources of error contributing to the observed variability. A statistical analysis is also difficult because different sources of error become important for light measurements done close to the sediment surface compared to light measurements in deeper sediment layers.

At the sediment surface, small deviations in measuring angle could result in large variations of the measured downwelling radiance because of the highly directional downwelling light field (solid lines in Fig. 4A,C,E). Measurements of upwelling radiance are less critical with respect to angular deviation caused by the isotropic distribution of upwelling light from the sediment surface (dashed lines in Fig. 4A,C,E). As the angular distribution of light becomes more isotropic with depth, angular deviations are less important in deeper sediment layers (Fig. 4B,D,F).

Other sources of error were a result of the small size of the fiber-optic microprobes, which was comparable to the size of the sediment particles. Therefore, the measurement resolution cannot be much better than half the average grain size of the sediment. Light was attenuated exponentially in deeper sediment layers (Figs. 3, 5, 6), and small deviations in depth scale could thus result in large deviations between repeated measurements. This effect becomes most important in sediments or sediment layers with high attention coefficients. The presence or absence of a sediment particle immediately in front of the optical fiber tip at the sediment surface could mean >10-fold more or less forward-scattered light. Similarly, a dark-colored sand grain or a microalgal assemblage could alter the measured radiance strongly, increasing the random noise in the data.

As a result of the mentioned sources of error, we observed the highest variability in light measurements close to the sediment surface. Measurements of downwelling radiance at 0°, 20°, and 40° in the upper 0.5 mm of the sediment were most critical and exhibited relative standard deviations of up to 50–80%. Both up- and downwelling light in deeper sediment layers as well as measurements of upwelling radiance at the sediment surface exhibited a significantly lower variability, and relative standard deviations ranged from <10 to 40%. The standard deviation is related to the arithmetic mean of multiple measurements. The nature of the mentioned sources of error do, however, have a multiplicative rather than additive effect on the observed variability of radiance data. Calculations of average radiance data were therefore performed on log-transformed data, and average radiance was thus calculated as the geometric mean of 2–5 measurements. This partly truncated the effects of outliers, as the geometric mean weights very small and very large values more equally than the traditional arithmetic mean does.

Direct measurements of scalar irradiance with a spherical microsensor also exhibited the highest variability (relative standard deviation of 30–40%) close to the sediment surface, where small differences in the surface topography and

composition of sand grains could have a large effect on the local light field (Fig. 5B). This effect of heterogeneity was, however, smoothed out to a certain degree because the scalar irradiance probe collects light via a diffusing sphere which integrates light from all directions. Uncertainties in the positioning of the probe were low because the scalar irradiance probe was inserted into the sediment from above while the sediment was being observed under a dissection microscope.

Modeling the light field in sediments—Measurements of the angular field radiance distribution provide the essential data for calculating all relevant light field parameters in sediments. Some of these parameters (e.g. irradiance and scalar irradiance, Kühl et al. 1994*a*) can also be measured directly. Although the absorption coefficient can be estimated by Gershun's equation (Eq. 11) from measured light field parameters, other important inherent optical parameters cannot be calculated without knowledge of the volume-scattering function. On the basis of experimental data or on Monte Carlo computer simulations using a representative volume-scattering function, empirical relations have been determined between measured light field parameters of the asymptotic light regime and inherent optical parameters of different water types (e.g. Herman and Lenoble 1964; Timofeeva 1974; Kirk 1981, 1991). A more analytical approach based on asymptotic closure theory was presented by Zaneveld (1989). These approaches cannot, however, be directly applied in sediments, where multiple scattering predominates.

Sediments are composed of randomly distributed particulate absorbers and scatterers of different composition that exhibit macroheterogeneity of refractive index relative to the surrounding water or air. The presence of discrete particles in a turbid medium rather than a homogeneous solution results in a distributional error on absorption measurements (Fukshansky 1987). In our study, the absorption coefficient for 650-nm light was higher in dry quartz sand than in wet sand, although measurements were performed in exactly the same material (Table 2). The different absorption coefficients found in dry and wet quartz sand could be due to such an effect of macroheterogeneity in combination with a shift in refractive index of the surrounding medium. Estimates of sediment absorption spectra by use of Eq. 11 should therefore be interpreted with care even though the calculations were done with asymptotic values for the relevant light field parameters that were obtained far from the sample boundaries.

An important effect of distributional error and multiple scattering is an apparent smoothing of measured absorption spectra (Fukshansky et al. 1993). The effect is due to a difference in pathlength travelled by photons per vertical distance traversed (being higher for photons at wavelengths with low absorption than for photons at wavelengths that are strongly absorbed within the first few encounters with a particle). Photons at wavelengths exhibiting a low probability for absorption upon a single encounter with a particle are subject to multiple scattering events, which increase their pathlength and therefore the probability for their absorption in a sediment layer. The resulting apparent higher absorption coefficient at these wavelengths would thus be due mainly to multiple scattering rather than reflecting "true" absorption characteristics of the medium. A rigorous analysis of the distributional error and possible corrections for this effect in turbid media by the combined use of radiative transfer and absorption statistics theory has been described by Fukshansky (1987) and Fukshansky et al. (1993).

In the case of laminated sediments, microbial mats, or biofilms, which are densely populated by phototrophic microorganisms, the degree of heterogeneity is even more pronounced. These communities often exhibit a multilayered structure due to the presence of different groups of phototrophic microalgae and bacteria, each with its own characteristic absorption spectrum. Consequently, a nonrandom variation with depth of the spectral absorption and scattering characteristics is observed (Jørgensen and Des Marais 1988; Pierson et al. 1990). Differences in structure between the single layers can also result in a discontinuity of the refractive index with depth leading to abrupt changes in the ratio of up- and downwelling light at the boundaries. Such a shift in the ratio between up- and downwelling irradiance in laminated sandy sediments was reported by Pierson et al. (1990). Finally, the high density of photopigments in these microbenthic communities means that fluorescence may become an important term for radiative transfer (*see Eq. 9*).

It can be concluded that sediments and microbial mats are macroheterogeneous multiple-scattering media with nonuniformly-spaced absorbers and scatterers. In such media, the use of the traditional radiative transfer theory (RTT) becomes questionable. An extension of the RTT has been presented by Anisimov and Fukshansky (1992). This *stochastic radiative transfer theory* treats the inherent optical parameters as stochastic variables which exhibit random fluctuations and can be characterized by a mean value, variances, and other statistical parameters. Whether the traditional RTT or the stochastic RTT can be applied in sediments is a very interesting theoretical problem, which is, however, outside the scope of our study. We present our data organized in the framework of the general notion of radiative transfer theory. The only information derived from the traditional RTT, however, is the absorption coefficient calculated by Gershun's law (Eq. 11). The use of Gershun's equation for calculating sediment absorption coefficients remains questionable, and additional theoretical analysis is necessary.

Models taking heterogeneity, refractive index mismatch, and fluorescence effects into account have been developed for light propagation in plant tissue, which exhibits a similar degree of complexity as microbenthic communities do (Fukshansky and Kazarinova 1980; Fukshansky-Kazarinova et al. 1986; Fukshansky et al. 1993; Anisimov and Fukshansky 1992). An important prerequisite for these models is detailed knowledge about the light field in plant tissue obtained primarily by use of fiber-optic microsensors (Vogelmann 1986; Vogelmann et al. 1991; Martinez v. Remisowsky et al. 1992). A similar approach seems promising for modeling the light field in microbenthic communities. Together with independent measurements of inherent optical parameters, fine-scale measurements of the light field along the lines presented here may therefore provide important data for developing appropriate models of light propagation in microbenthic communities.

Conclusions

By using fiber-optic microprobes to measure radiance distributions, it is now possible to obtain detailed information about the light field in microbenthic communities and about the physical mechanisms behind observed optical phenomena. In uniform sediment layers, a transition from an anisotropic light field near the sediment surface to an asymptotic light field in deeper sediment layers occurs within the upper millimeter of the sediment. The near-surface light field is strongly determined by the microscale optics of the interface between sediment and overlying air or water, where a combination of diffuse backscattered and internally reflected light results in a higher total light intensity than the incident light. In the presence of selective absorption by photopigments, these mechanisms also result in a significant alteration in the spectral composition of total light available for photobiological processes as compared to incident light.

Furthermore, the combined action of multiple scattering and absorption results in steep light gradients exhibiting high attenuation coefficients with depth. All of these effects are of paramount importance in photobiological studies of sediment communities. Relating microbenthic photosynthesis to downwelling radiance or irradiance without taking the importance of scattered light into account may result in serious errors. Quantitative studies of light and photosynthesis in microbenthic communities (e.g. action spectra and light saturation studies of photosynthesis) should therefore include direct light measurements of spectral scalar irradiance with a spherical fiber-optic microprobe.

Microbenthic communities exhibit various levels of optical complexity. The theoretical understanding and modeling of the light field in microbenthic communities must therefore take the importance of both multiple scattering and heterogeneity with respect to particle distribution and composition into account. Such models have recently been developed for light propagation in animal and plant tissue but have not yet been applied to sediments.

References

ANDERSON, R. R., AND OTHERS. 1989. Pulsed photothermal radiometry in turbid media: Internal reflection of backscattered radiation strongly influences optical dosimetry. Appl. Opt. **28**: 2256–2262.

ÅNGSTRÖM, A. 1925. The albedo of various surfaces of the ground. Geogr. Ann. **7**: 323–342.

ANISIMOV, O., AND L. FUKSHANSKY. 1992. Stochastic radiation in macroheterogeneous random optical me-

dia. J. Quant. Spectrosc. Radiat. Transfer **48:** 169–186.

ASHLEY, L. E., AND C. M. COBB. 1958. Single particle scattering functions for latex spheres in water. J. Opt. Soc. Am. **48:** 261–268.

BLISS, D., AND H. SMITH. 1985. Penetration of light into soil and its role in the control of seed germination. Plant Cell Environ. **8:** 475–483.

BOHREN, C. F. 1983. Multiple scattering at the beach. Weatherwise **36:** 197–200.

———. 1988. Understanding color in nature. Pigment Cell Res. **1:** 214–222.

CHEONG, W. F., S. A. PRAHL, AND A. J. WELCH. 1990. A review of the optical properties of biological tissues. IEEE J. Quant. Electron. **26:** 2166–2185.

FENCHEL, T., AND B. J. STRAARUP. 1971. Vertical distribution of photosynthetic pigments and the penetration of light in marine sediments. Oikos **22:** 172–182.

FUKSHANSKY, L. 1987. Absorption statistics in turbid media. J. Quant. Spectrosc. Radiat. Transfer **38:** 389–406.

———, N. FUKSHANSKY-KAZARINOVA, AND A. MARTINEZ V. REMISOWSKY. 1991. Estimation of optical parameters in a living tissue by solving the inverse problem of the multi-flux radiative transfer. Appl. Opt. **30:** 3145–3153.

———, AND N. KAZARINOVA. 1980. Extension of the Kubelka-Munk theory of light propagation in intensely scattering materials to fluorescent media. J. Opt. Soc. Am. **70:** 1101–1111.

———, AND OTHERS. 1993. Absorption spectra of leaves corrected for scattering and distributional error: A radiative transfer and absorption statistics treatment. Photochem. Photobiol. **57:** 538–555.

FUKSHANSKY-KAZARINOVA, N., W. LORK, E. SCHAFER, AND L. FUKSHANSKY. 1986. Photon flux gradients in layered turbid media: Application to biological tissues. Appl. Opt. **25:** 780–788.

GERSHUN, A. 1939. The light field. J. Math. Phys. **18:** 51–153.

GOMOIU, M. T. 1967. Some quantitative data on light penetration in sediments. Helgol. Wiss. Meeresunters. **15:** 120–127.

GROENHUIS, R. A. J., H. A. FERWERDA, AND J. J. TEN BOSCH. 1983. Scattering and absorption of turbid materials determined from reflection measurements. 1: Theory. Appl. Opt. **22:** 2456–2462.

HAARDT, H., AND G. Æ. NIELSEN. 1980. Attenuation measurements of monocromatic light in marine sediments. Oceanol. Acta **3:** 333–338.

HERMAN, M., AND J. LENOBLE. 1964. Etude du regime asymptotique dans un milieu diffusant et absorbant. Rev. Opt. **43:** 555–572.

HODKINSON, J. R., AND J. I. GREENLEAVES. 1963. Computations of light-scattering and extinction by spheres according to diffraction and geometrical optics and some comparisons with the Mie theory. J. Opt. Soc. Am. **53:** 577–588.

HOFFMANN, C. 1949. Über die Durchlässigkeit dünner Sandschichten für Licht. Planta **36:** 48–56.

HØJERSLEV, N. K. 1986. Optical properties of sea water, p. 383–462. *In* J. Sündermann [ed.], Oceanography. V. 3. Landolt-Börnstein/Springer.

IAPSO. 1985. The international system of units (SI) in oceanography. UNESCO Tech. Pap. Mar. Sci. 45. 124 p.

ISACCHI, S., AND J. LENOBLE. 1959. Etude experimentale des diffusions multiples de la lumiere. Rev. Opt. **38:** 217–237.

ISHIMARU, A. 1978. Wave propagation in random media. V. 1. Academic.

———. 1989. Diffusion of light in turbid material. Appl. Opt. **28:** 2210–2215.

JERLOV, N. G. 1976. Marine optics. Elsevier.

JØRGENSEN, B. B. 1989. Light penetration, absorption and action spectra in cyanobacterial mats, p. 123–137. *In* Y. Cohen and E. Rosenberg [eds.], Physiological ecology of benthic microbial communities. Am. Soc. Microbiol.

———, AND D. J. DES MARAIS. 1986. A simple fiber-optic microprobe for high resolution light measurements: Application in marine sediment. Limnol. Oceanogr. **31:** 1376–1383.

———, AND ———. 1988. Optical properties of benthic photosynthetic communities: Fiber-optic studies of cyanobacterial mats. Limnol. Oceanogr. **33:** 99–113.

———, N. P. REVSBECH, AND Y. COHEN. 1983. Photosynthesis and structure of benthic microbial mats: Microelectrode and SEM studies of four cyanobacterial communities. Limnol. Oceanogr. **28:** 1075–1093.

KAUFMANN, W. F., AND K. M. HARTMANN. 1988. Internal brightness of disk-shaped samples. J. Photochem. Photobiol. B: Biol. **1:** 337–360.

KIRK, J. T. O. 1981. Monte Carlo study of the nature of the underwater light field in, and the relationship between optical properties of, turbid yellow waters. Aust. J. Mar. Freshwater Res. **32:** 517–532.

———. 1983. Light and photosynthesis in aquatic ecosystems. Cambridge.

———. 1991. Volume scattering function, average cosines, and the underwater light field. Limnol. Oceanogr. **36:** 455–467.

KORTÜM, G. 1969. Reflectance spectroscopy. Springer.

KÜHL, M., AND B. B. JØRGENSEN. 1992. Spectral light measurements in microbenthic communities with a fiber-optic microprobe coupled to a sensitive diode array detector system. Limnol. Oceanogr. **37:** 1813–1823.

———, C. LASSEN, AND B. B. JØRGENSEN. 1994*a*. Light penetration and light intensity in sandy marine sediments measured with irradiance and scalar irradiance fiber-optic microprobes. Mar. Ecol. Prog. Ser. **105:** 139–148.

———, ———, AND ———. 1994*b*. Optical properties of microbial mats: Light measurements with fiber-optic microprobes, p. 149–166. *In* L. J. Stal and P. Caumette [eds.], Microbial mats: Structure, development and environmental significance. NATO ASI Ser. G. Springer.

KULLENBERG, G. 1972. Observed and computed scattering functions, p. 25–49. *In* N. G. Jerlov and E. Steemann Nielsen [eds.], Optical aspects of oceanography. Academic.

LASSEN, C., H. PLOUG, AND B. B. JØRGENSEN. 1992*a*. A fibre-optic scalar irradiance microsensor: Application for spectral light measurements in sediments. FEMS (Fed. Eur. Microbiol. Soc.) Microbiol. Ecol. **86:** 247–254.

———, ———, AND ———. 1992*b*. Microalgal photosynthesis and spectral irradiance in coastal marine sediments of Limfjorden, Denmark. Limnol. Oceanogr. **37:** 760–772.

LEKNER, J., AND M. C. DORF. 1988. Why some things are darker when wet. Appl. Opt. **27:** 1278–1280.

MANDOLI, D. F., G. A. FORD, L. J. WALDRON, J. A. NEMSON, AND W. R. BRIGGS. 1990. Some spectral properties of several soil types: Implications for photomorphogenesis. Plant Cell Environ. **13:** 287–294.

MARTINEZ V. REMISOWSKY, A., J. MCCLENDON, AND L. FUKSHANSKY. 1992. Estimation of the optical parameters and light gradients in leaves: Multi-flux versus two-flux treatment. Photochem. Photobiol. **55:** 857–865.

MOES, C. J. M., M. J. C. VAN GEMERT, W. M. STAR, J. P. A. MARIJNISSEN, AND S. A. PRAHL. 1989. Measurements and calculations of the energy fluence rate in a scattering and absorbing phantom at 633 nm. Appl. Opt. **28:** 2292–2296.

MOTAMEDI, M., S. RASTEGAR, G. LECARPENTIER, AND A. J. WELCH. 1989. Light and temperature distribution in laser irradiated tissue: The influence of anisotropic scattering and refractive index. Appl. Opt. **28:** 2230–2237.

PIERSON, B. K., V. M. SANDS, AND J. L. FREDERICK. 1990. Spectral irradiance and distribution of pigments in a highly layered marine microbial mat. Appl. Environ. Microbiol. **56:** 2327–2340.

PREISENDORFER, R. W. 1959. Theoretical proof of the existence of characteristic diffuse light in natural waters. J. Mar. Res. **18:** 1–9.

———. 1976. Hydrologic optics. V. 1–6. NTIS, Springfield.

PROFIO, A. E. 1989. Light transport in tissue. Appl. Opt. **28:** 2216–2222.

REVSBECH, N. P., AND B. B. JØRGENSEN. 1983. Photosynthesis of benthic microflora measured with high spatial resolution by the oxygen microprofile method: Capabilities and limitations of the method. Limnol. Oceanogr. **28:** 749–756.

SELLERS, W. D. 1965. Physical climatology. Univ. Chicago.

SMITH, R. C., AND W. H. WILSON. 1972. Photon scalar irradiance. Appl. Opt. **11:** 934–938.

STAR, W. M., J. P. A. MARIJNISSEN, AND M. J. C. VAN GEMERT. 1987. Light dosimetry: Status and prospects. J. Photochem. Photobiol. Ser. B **1:** 149–167.

TAYLOR, W. R. 1964. Light and photosynthesis in intertidal benthic diatoms. Helgol. Wiss. Meeresunters. **10:** 29–37.

———, AND C. D. GEBELEIN. 1966. Plant pigments and light penetration in intertidal sediments. Helgol. Wiss. Meeresunters. **13:** 229–237.

TESTER, M., AND C. MORRIS. 1987. The penetration of light through soil. Plant Cell Environ. **10:** 281–286.

TIMOFEEVA, V. A. 1974. Optics of turbid waters (results of laboratory studies), p. 177–219. *In* N. G. Jerlov and E. Steemann Nielsen [eds.], Optical aspects of oceanography. Academic.

TWOMEY, S. A., C. F. BOHREN, AND J. L. MERGENTHALER. 1986. Reflectance and albedo differences between wet and dry surfaces. Appl. Opt. **25:** 431–437.

TYLER, J. E. 1960. Radiance distribution as a function of depth in an underwater environment. Bull. Scripps Inst. Oceanogr. **7:** 363–411.

———, W. H. RICHARDSON, AND R. W. HOLMES. 1959. Method for obtaining the optical properties of large bodies of water. J. Geophys. Res. **64:** 667–673.

VAN DE HULST, H. C. 1957. Light scattering by small particles. Wiley.

VOGELMANN, T. C. 1986. Light within the plant, p. 307–337. *In* R. E. Kendrick and G. H. M. Kronenberg [eds.], Photomorphogenesis in plants. Martinus-Nijhoff.

———, AND L. O. BJÖRN. 1984. Measurements of light gradients and spectral regime in plant tissue with a fiber optic probe. Physiol. Plant. **60:** 361–368.

———, G. MARTIN, G. CHEN, AND D. BUTTRY. 1991. Fibre optic microprobes and measurement of the light microenvironment within plant tissues. Adv. Bot. Res. **18:** 255–295.

WILSON, B. C., AND S. L. JAQUES. 1990. Optical reflectance and transmittance of tissues: Principles and applications. IEEE J. Quant. Electron. **26:** 2186–2199.

WOOLLEY, J. T., AND E. W. STOLLER. 1978. Light penetration and light-induced seed germination in soil. Plant Physiol. **61:** 597–600.

ZANEVELD, J. R. V. 1989. An asymptotic closure theory for irradiance in the sea and its inversion to obtain the inherent optical properties. Limnol. Oceanogr. **34:** 1442–1452.

Submitted: 15 March 1993
Accepted: 27 January 1994
Amended: 16 March 1994